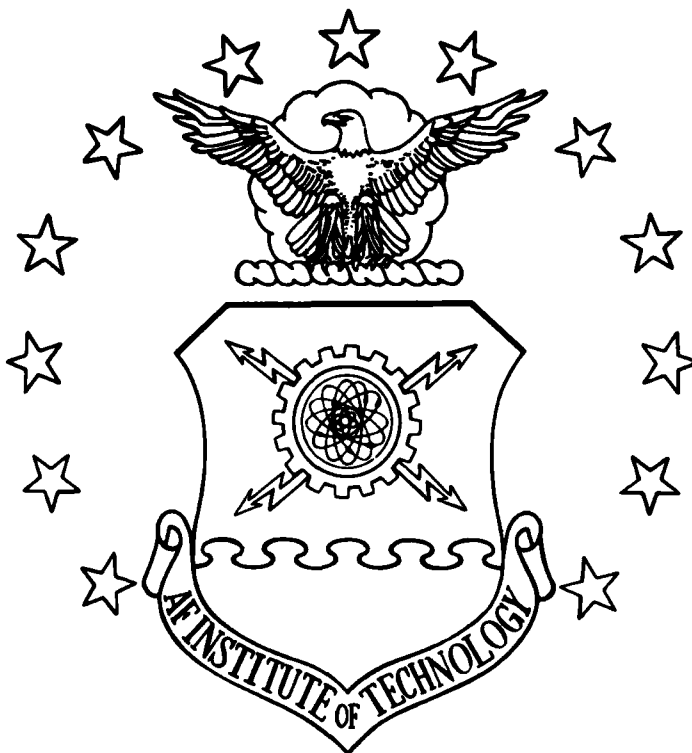
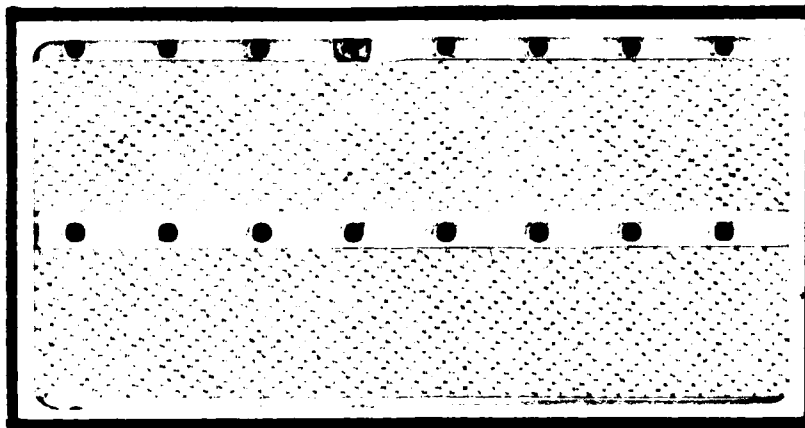


AD-A159 214



DTIC FILE COPY



This document has been approved
for public release and sale; its
distribution is unlimited.

DTIC
ELECTRONIC
SEP 18 1985
S
A
D

DEPARTMENT OF THE AIR FORCE
AIR UNIVERSITY
AIR FORCE INSTITUTE OF TECHNOLOGY

Wright-Patterson Air Force Base, Ohio

85 09 17 033

AFIT/GNE/ENP/85M-6

MACH STEM MODELING WITH SPHERICAL

SHOCK WAVES

THESIS

William E. Eichinger
Captain US Army

AFIT/GNE/ENP/85M-6

DTIC
ELECTRONIC
S SEP 18 1985 D
A

Approved for Public Release; Distribution Unlimited

MACH STEM MODELING WITH SPHERICAL
SHOCK WAVES

THESIS

Presented to the Faculty of the School of Engineering
of the Air Force Institute of Technology
Air University
in Partial Fulfillment of the
Requirements for the Degree of
Master of Science

by
William E. Eichinger
Captain, US Army Corps of Engineers
Graduate Nuclear Engineering
March 1985

Accession For	
NTIS GRA&I	<input checked="" type="checkbox"/>
DTIC TAB	<input type="checkbox"/>
Unannounced	<input type="checkbox"/>
Justification	
By _____	
Distribution/	
Availability Codes	
Dist	Avail and/or Special
A-1	



PREFACE

This paper is dedicated to the memory of my son, Brian Jon Eichinger.

The purpose of this study was to find a method of predicting the environment in the path of a Mach stem in a nuclear explosion. There are many indications of the inadequacy of present modeling methods. The prediction method and program in Appendix F is intended to be simple, but accurate. As the study progressed it became obvious that the Mach stem phenomenon is a dynamic process that changes throughout its life. Thus to adequately describe the conditions would require an inordinate amount of equations. This study is self-limited to the region of interest of survivability studies of aircraft.

In performing this study, I am deeply indebted to Major Larry McKee, my advisor, for his assistance and guidance. I also wish to thank Dr. George Ulrich of the Defense Nuclear Agency and Mr. Ray Ruetnick for their advice and help. Finally, I wish to thank my wife Leanne and daughter Heidi for their patience and understanding during this period.

William E. Eichinger

CONTENTS

	<u>Page</u>
Preface - - - - -	ii
List of Figures - - - - -	v
List of Tables - - - - -	vi
Abstract - - - - -	vii
Notation - - - - -	viii
I. Introduction - - - - -	1
II. Mach Effect - - - - -	3
III. Oblique Shock Reflection Theory - - - - -	8
Use of Planar Shocks for Spherical Shocks - -	8
Two Shock Theory - - - - -	10
Three Shock Theory - - - - -	15
IV. Prediction of the Path of the Triple Point - -	20
Prediction by Theory - - - - -	20
Strong Shock Solution - - - - -	21
Use of Experimental Data - - - - -	27
Solution for Heights Greater than HOB - - - -	28
Comparison to Nuclear Explosions - - - - -	32
V. Empirical Results for Shape, Ta, and Overpress- 37	
Shape and Orientation of the Wave - - - - -	37
Time of Arrival - - - - -	41
Overpressure - - - - -	43
Example Problem - - - - -	54
Comparison to Traditional Methods - - - - -	56
VII. Conclusions and Recommendations - - - - -	61
Bibliography - - - - -	65

APPENDICES

Appendix A: Oblique Shock Relations - - - - - 71
Appendix B: Mach Stem Overpressure Data - - - - - 73
Appendix C: Origin of the Triple Point Data - - - - 78
Appendix D: Ground Overpressure Data - - - - - 80
Appendix E: Nuclear Explosion Parameters - - - - - 81
Appendix F: Program Description - - - - - 82
Vita - - - - - 93

List Of Figures

Figure

1. Mach Stem Formation - - - - -	4
2. Shock Wave Contours - - - - -	5
3. Precursor Structure - - - - -	5
4. Spherical Shock Configuration - - - - -	9
5. Planar Shock Configuration - - - - -	9
6. Regular Reflection - - - - -	10
7. Variation of Extreme Angle with Strength - - - -	14
8. Mach Stem Configuration - - - - -	16
9. Comparison of Two and Three Shock Theory Exper. -	19
10. Regions and Angles for Strong Shock Relations -	22
11. Shock Configuration in Frame of Triple Point - -	23
12. Shock Configuration at Late Times - - - - -	29
13. Planar Approximation - - - - -	29
14. Triple Point Trajectory Comparison 135' HOB - -	34
15. Triple Point Trajectory Comparison 700' HOB - -	35
16. Variation of Mach Stem Shape with Time - - - - -	38
17. Airflow near Triple Point, HTP Greater than HOB	40
18. Variation of Pressure with Distance up Mach Stem	46
19. Variation of ψ with Mach Number - - - - -	49
20. Pressure Increase in Mach Stem Vs. Time - - - -	48
21. Iso-Overpressure Contour 200' SHOB - - - - -	57
22. Iso-Overpressure Contour Comparison - - - - -	58
23. Iso-Overpressure Contour Comparison - - - - -	59

List of Tables

Table

1. Effective Radius of Mach Stem - - - - - 40
2. Comparison of Time of Arrival Equations - - - - - 43

Abstract

A semiempirical model was developed for the treatment of the Mach stem region of a nuclear airburst. This model predicts the conditions that would be observed by an aircraft or missile as well as the limits of this region in space. The model is based upon current shock theory. Where three shock theory fails to accurately predict physical reality, new relations are developed or empirical data is used.

Specifically, this model predicts the path of the triple point, the overpressure, dynamic pressure, time of arrival, and direction of the shock impulse above the ground. An explanation of the development of each prediction is made and compared to actual nuclear or high explosive test data. Additionally, a comparison is made between conventional Mach stem modeling and this model.

Unique to this model is a method of predicting the variation of pressure with altitude above the ground. For low scaled heights of burst, the overpressure found at an altitude of 20⁹/₈ percent of the triple point height is greater than that on the ground. In addition, the overpressure measured just below the triple point is found to be only 60⁹/₈ percent of the ground overpressure scaled to altitude. This prediction is radically different than conventional ground overpressures scaled to atmospheric pressure at altitude. The predictions made by this model are verified by nuclear and high explosive test data. (10000)

NOTATION

Air Zero	Point of detonation of the weapon
Ground Zero	Ground location directly below the burst
HOB	Height of the burst above the ground
HTP	Height of the triple point above the ground
Incident Shock	Shock wave generated directly from a burst
M	Mach number
OTP	Origin of the triple point, the ground distance at which the Mach shock begins to form
P	Pressure (psi.)
dP	Overpressure
Reflected Shock	Shock wave generated by reflection of the incident
Ta	Time of arrival of the shock wave (sec.)
Triple Point	Point of intersection of the incident, Mach and reflected shocks.
U	Velocity
α	Angle of incidence
γ	Ratio of specific heats--equal to 1.4 for air
δ	Angle of deflection of gas through a shock
θ	Wedge angle
ξ	Shock strength as defined by $P_o/(P_o + dP)$
ρ	Density
τ	Direction of the gust loading of airfoils
ϕ	Angle between flow of air and shock
ψ	Triple point trajectory angle
Subscripts 1,2,3,4	Denotes region of measurement

I. Introduction

It can be shown that air bursts are most effective in attacking soft or moderately hard targets with nuclear weapons. Further, surface bursts loft great quantities of dust and debris into the atmosphere. This material can be exceedingly damaging to subsequent warheads targeted in the vicinity of the first blast. Thus it is likely that airbursts will be used against many military and civilian targets. This paper deals with air blast phenomenon in the Mach stem region of the blast wave emanating from a nuclear weapon. The Mach stem is an effect that occurs in near surface bursts (less than 1000 Scaled Feet) and which can reach up to five miles in height. It is thus important in survivability studies of airborne vehicles such as aircraft and launching missiles.

Presently, the overpressure in the Mach stem is assumed to be constant vertically and is scaled only by the variation of pressure due to the altitude of the target (19:2-50). It is further assumed that the Mach stem is vertical to the ground at all altitudes. This leads to the assumption that the impulse which is delivered to a target in the Mach stem is parallel to the ground. The time at which the Mach stem blast wave arrives at a target above the ground is not addressed at all. A cursory examination of photographs of near surface nuclear bursts clearly shows that the Mach stem is in general not vertical. Changes in curvature in the Mach stem are an indication that the overpressure in the Mach stem is not constant over the entire vertical distance of the shock.

There are several works that treat the phenomena of nuclear bursts.

The most important of these are the Defense Nuclear Agency manual EM-1, Glasstone's Effects of Nuclear Weapons, and the Defense Atomic Support Agency manuals DASA-1200 and DASA-2506. Amongst these manuals, blast effects are treated in great detail. However, the conditions that are to be found in the path of the Mach stem above the surface of the earth are not discussed. In order to develop a model which will predict blast parameters this paper will:

1. Examine current theory of shock reflection.
2. Use the results of current theory to predict the path of the triple point.
3. Examine nuclear blast data to find relations for the shape, time of arrival, and overpressure of the shock at altitude.
4. Compare predictions made by the resulting relations to other predictions and experimental data.

II. Mach Effect

The Mach stem was first discovered in 1878 by the pioneer researcher Ernst Mach for whom it was named. It remained obscure until 1941 when Von Neumann introduced the first analytical criterion on how the phenomenon occurs. During the Second World War, American scientists studied the effect and discovered that the destructive effects of bombs could be increased by exploding the weapon at some height above the ground. The blast overpressure as measured at a fixed location on the ground increased as the height of detonation increased until an ideal height was reached and then decreased with higher heights of burst. This increase in overpressure is caused by the formation of a Mach stem at certain ranges and overpressures (17:1). When the early nuclear tests were done in the mid-1950's, investigations were conducted to determine if the same effects occurred in nuclear weapons as well. The tests showed that, with proper scaling, nuclear weapons exhibit the same blast characteristics as conventional weapons.

When a nuclear weapon is detonated at some height above the surface of the earth, a spherical blast wave is emitted from the device. This wave strikes the ground at an angle of incidence that grows from zero to 90 degrees for locations away from ground zero. The angle of incidence is defined as the angle between the tangent to the shock and the ground.

A reflected shock wave is formed which travels behind the incident wave. Because the air behind the incident wave is hotter and more dense than the air in front of it, the reflected wave travels faster than the

incident wave. Under certain conditions, the reflected wave may catch up to the incident wave, merge with it and thus reinforce the incident shock wave (See figure 1). The region in which there is a separate and distinct reflected shock is called the regular reflection region. The region where the shock wave is reinforced by the reflected wave is called the irregular or Mach reflection region. The top of the Mach stem is called the triple point. At this point, three shocks (the Mach stem, the incident wave, and the reflected wave) converge.

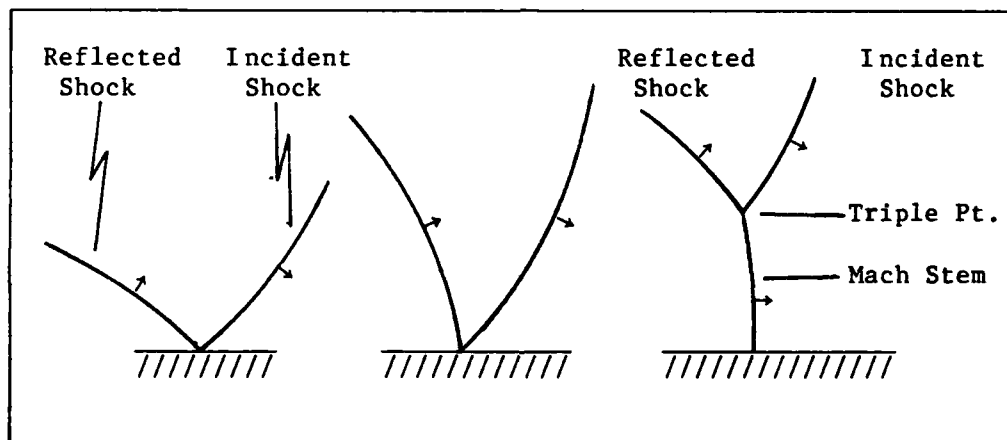
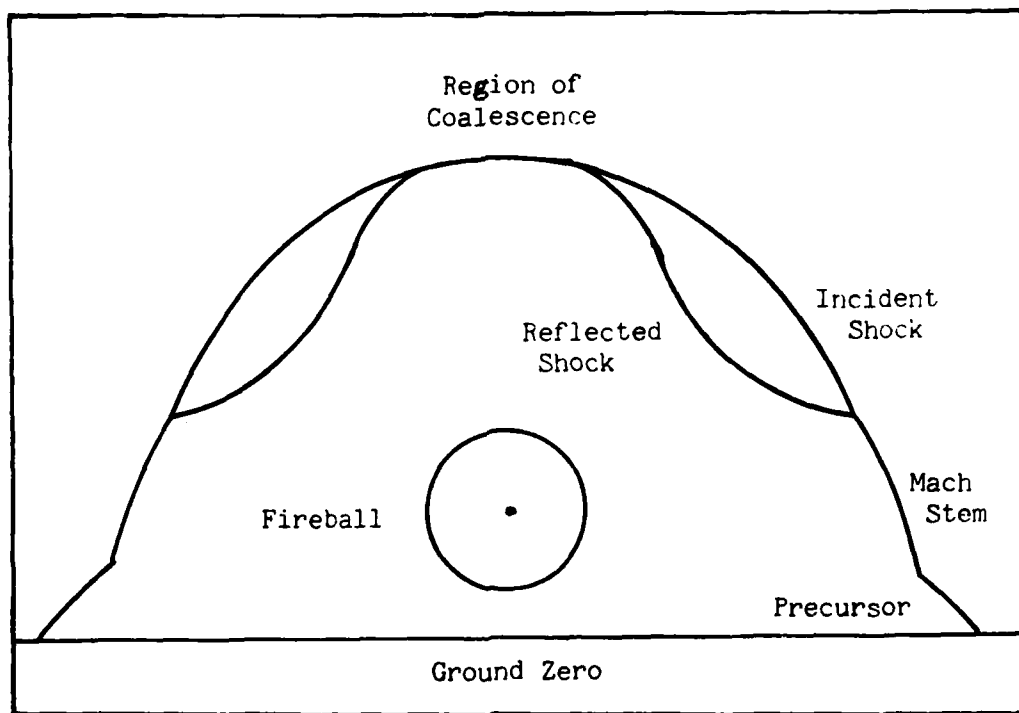


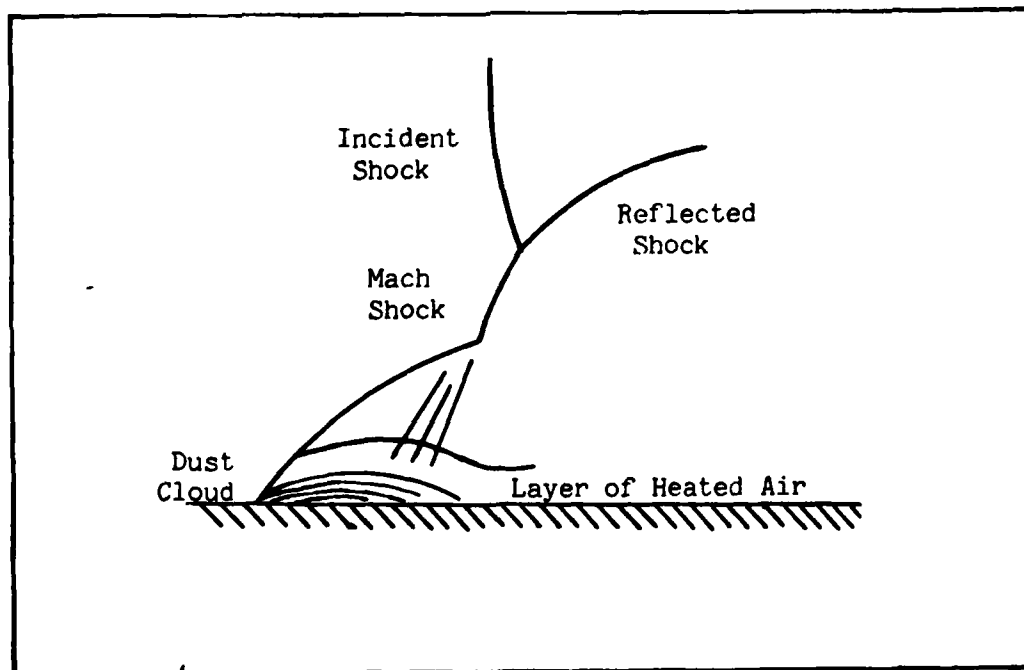
Figure 1. Mach Stem Formation

Several other effects have been observed in the nuclear weapons tests. For low scaled heights of burst (less than 200 feet), a substantial portion of the reflected wave must travel through the region of the expanding fireball. The air in this area has been heated to extremely hot temperatures (7000 degrees K.) (27:307). This causes the reflected shock wave to be refracted as it passes through the region. The net effect of this refraction is to weaken the reflected shock and to increase its velocity in the vertical direction (See figure 2). The



(46:44)

Figure 2. Shock Wave Contours



(63:13)

Figure 3. Precursor Structure

velocity of the reflected wave may be increased to the point that the part which passed through the fireball overtakes the incident wave. Under normal conditions, the reflected wave would overtake the incident wave close to the ground first, forming a Mach stem. For low heights of burst, the reflected wave above the fireball overtakes the incident wave and forms a second Mach stem directly over the burst. The size of this region of coalescence can be estimated using techniques described in DASA-1200 (22:4-177). However, since the reflected wave is greatly weakened by the passage through the fireball, the effect of its reinforcement of the incident shock is minimal. In the Teapot series of tests, for example, this closure was seen on two of the tests, numbers 4 and 12. On shot 12, there was no perceptible reinforcement of the incident wave at all in the region directly above the burst. On shot 4, the coalescence of the waves corresponded to an increase in effective yield of only 16 percent (46:42-45,76-79). For an ideal Mach stem formed above a perfectly reflecting plane, the increase in effective yield would be 100 percent. Because the effect of the closure of the shock waves above the burst does not greatly increase the threat to aircraft it will not be examined in this paper.

The radiation emanating from a nuclear weapon can also cause a phenomenon known as a precursor. This radiation heats the air near the ground, causing the incident wave to travel faster. A toe-shaped protuberance is formed on the incident shock wave near the ground. This is called the precursor (See figure 3). This effect is very complex and not well understood. There are great variations in overpressure with height in the precursor. This makes an accurate estimate of the actual

overpressure on the ground very difficult. The angle of incidence of the shock wave in the precursor region also changes dramatically (55:96-97). The precursor effect can mask the formation of the Mach stem in its early stages. For this reason, the actual origin of the triple point (the point at which the Mach stem begins to form) is not well known for many heights of burst. Because of the uncertainty of the conditions in the precursor region, it will not be considered in this study.

In recent years, laboratory experiments have discovered that there are several different forms of Mach reflection, namely single Mach reflection, complex Mach reflection, and double Mach reflection. The phenomenon observed at large distances (about equal to the HOB) is the single Mach reflection. At very close distances and high overpressures, complex Mach reflection and double Mach reflection may occur. These effects further increase the overpressure on the ground and thus may increase the danger to reinforced structures on the ground. Because this report primarily concerns the effects seen by airborne vehicles, the single Mach reflection will be assumed in all cases.

III. Oblique Shock Reflection Theory.

Use of Planar Shock Theory for Spherical Shocks.

Solving the fluid dynamic equations in a spherical geometry is an extremely difficult task both analytically and numerically. In order to simplify the problem, a spherical shock system is assumed to be instantaneously modeled as a planar system with a similar configuration. Thus the spherical shock system in figure 4 is assumed to be instantaneously equivalent to the planar system in figure 5. The angle of incidence of the spherical shock as measured by the tangent to the shock is the same as the angle of incidence in the planar shock. The wedge angle θ_w of the planar shock system is equivalent to the angle θ in figure 4. Once the pressure and triple point trajectory angle are determined for the planar system, they are assumed to be the same for the spherical system.

One series of calculations is sufficient to determine the configuration of the planar system. Because the configuration of the spherical system changes with time, it requires that many planar systems be solved in order to determine the characteristics of the spherical shocks with time. Solving these multiple problems will enable the prediction of the path of the triple point.

In order to formulate and solve the problem of oblique shock reflection, several assumptions were made. The medium in which the shock flows is a perfect diatomic gas. For this gas, gamma, the ratio of specific heats is equal to 1.4. This restriction can be later relaxed by

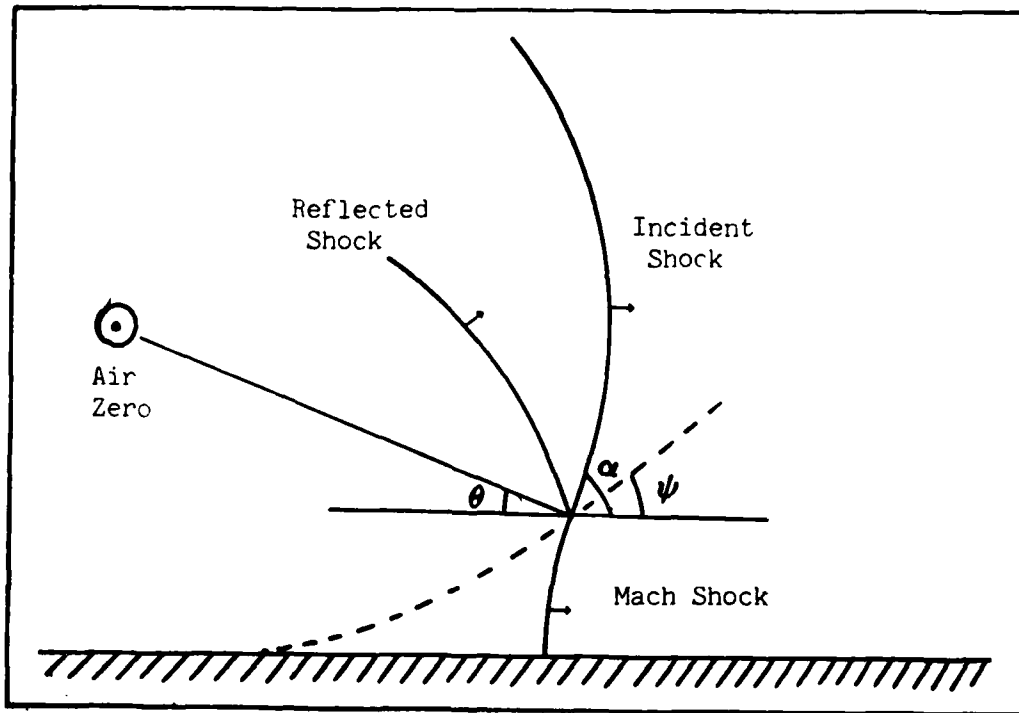


Figure 4. Spherical Shock Configuration

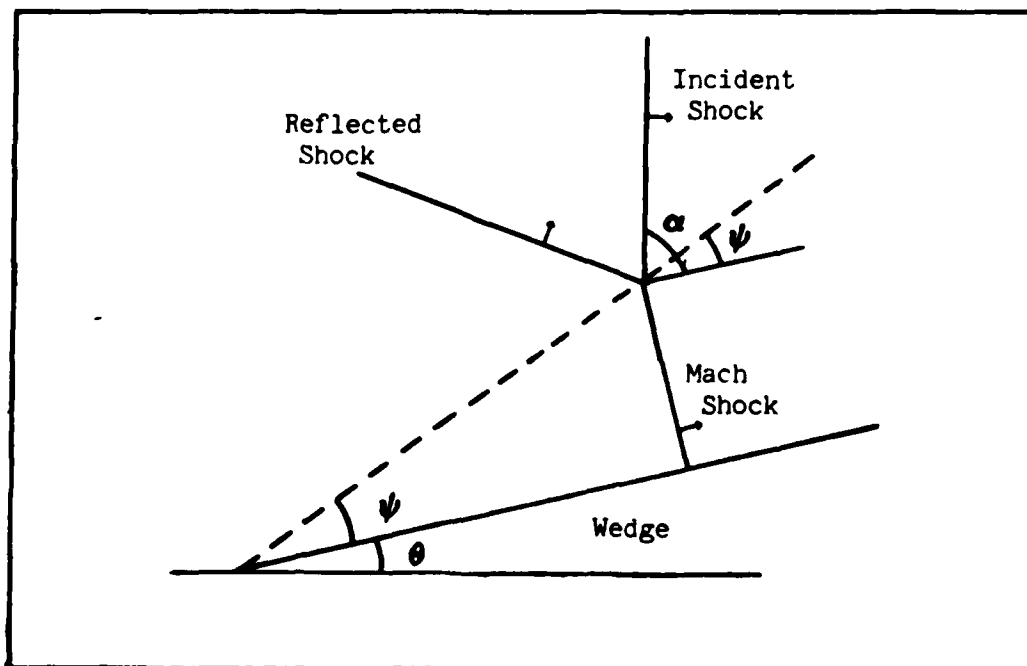


Figure 5. Planar Shock Configuration

assuming that gamma is a variable function of the incident overpressure. The second assumption is that all fluid flows are two-dimensional and inviscid. Flows are also assumed to be self-similar. That is, the three variables x , y , and t are not independent. The problem can be described at any point in terms of the new variables x/t and y/t . Thus the components of velocity in the x and y directions are constant. It is further assumed that when two shock solutions are possible, the weaker of the two solutions will be the physically correct one. Although it has never been proven, this experimental fact is assumed to be due to a requirement of minimum entropy (5:1,2).

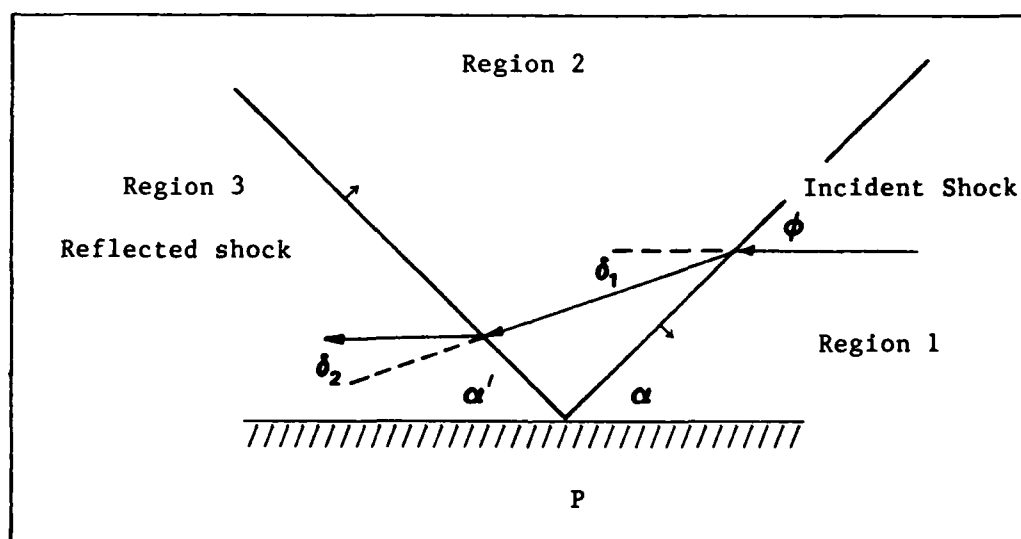


Figure 6. Regular Reflection
As Viewed in the Frame of Point P Stationary
(Incident Shock moving to the right)

Two Shock Theory.

Two shock theory deals with the reflection of an oblique shock wave from an ideal reflector. When an oblique shock wave strikes a surface, a

reflected wave is formed (See figure 6). The strength and angle of reflection may be found from the analysis of the air flow in the vicinity of the point of reflection (Designated P in figure 6). With respect to an observer traveling on the point of reflection, P, the ambient air (region 1) is flowing towards him with a velocity equal to $U_s/\sin\alpha$. The flow of air is depicted in figure 6 by arrows. The conditions across the shock from region 1 to region 2 are expressed by the following four equations which are statements of conservation of mass, momentum and energy: (5:8,9)

$$\rho_1 \tan\alpha = \rho_2 \tan(\alpha - \delta_1) \quad (\text{III-1})$$

$$\rho_1 U_1 \sin\alpha = \rho_2 U_2 \sin(\alpha - \delta_1) \quad (\text{III-2})$$

$$P_1 + \rho_1 U_1^2 \sin^2\alpha = P_2 + \rho_2 U_2^2 \sin^2(\alpha - \delta_1) \quad (\text{III-3})$$

$$H_1 + \frac{1}{2} U_1^2 \sin^2\alpha = H_2 + \frac{1}{2} U_2^2 \sin^2(\alpha - \delta_1) \quad (\text{III-4})$$

Where: ρ_1, ρ_2 are the air densities in regions 1 and 2.

U_1, U_2 are the velocities of air in regions 1 and 2

U_s is the velocity of the incident shock

P_1, P_2 are the pressures in regions 1 and 2.

α is the angle of incidence.

δ_1 is the angle of deflection of the incoming flow.

H_1, H_2 are the enthalpies of the air in regions 1 and 2.

A similar set of four equations can be written for the conditions across the reflected shock in going from region 2 to region 3. Because the flow near the wall must move parallel to the ground, the strength and angle of the reflected shock must be such that it causes a deflection of the flow through an angle equal in magnitude to the first deflection but

opposite in direction. That is:

$$\delta_2 = -\delta_1 \quad (\text{III-5})$$

These nine equations and the equation of state are sufficient to completely describe the conditions. Knowing the incident angle, the ambient air conditions, and the shock strength, one can solve for the reflected shock (5:9). As the angle of incidence increases, the magnitude of the reflected shock increases until at some angle the strength of the reflected shock is greater than that of the incident shock. Thus for an aircraft in this region, the reflected shock will be more damaging than the incident shock. The angle at which the reflected shock becomes greater than the incident shock is found from the relation:

$$\alpha = \frac{1}{2} \arccos[(\gamma - 1)/2] \quad (\text{III-6})$$

For ideal air with gamma equal to 1.4, this angle is 39.23 degrees (15:327). As the angle of incidence increases past this angle, the reflected shock increases in magnitude. In solving the above equations, one will find that there is no real solution to the problem for certain shock strengths and angles. These are the regions of Mach reflection. The angle at which Mach reflection begins for a given shock strength is called the extreme angle and is designated α_e . This angle can be found from the following relation (29:54):

$$[2x(\eta^2 x^2 + 1)]^2 - 4[[\gamma(\eta(1+x^2(\eta-1))-1) + \eta(1+x^2)]^2 - [\eta^2 x^2 + 1]^2] = 0$$

$$\text{Where } x = \tan(\pi/2 - \alpha_e) \quad (\text{III-7})$$

$$\eta = \frac{\rho_1}{\rho_2} = \left[\frac{\gamma+1}{\xi} + \gamma-1 \right] / \left[\frac{\gamma-1}{\xi} + \gamma+1 \right]$$

The origin of the triple point (OTP) is related to α_e by the following:

$$\text{OTP} = \text{HOBtan } \alpha_e \quad (\text{III-8})$$

Figure 7 is a graph of α_e versus the incident shock strength. Plotted as shown, the curve describes the boundary between the Mach reflection region and the regular reflection region. It should be noted that experiments have consistently shown that regular reflection persists several degrees beyond that which is predicted by this theory. The difference in predictions is less than four degrees except for shocks of strength $<.2$ (29:55). Shock strength is defined as the ratio of the pressure ahead of the shock to that behind it. Thus strength is always a number less than 1 and the stronger the shock, the lower the 'strength'. Note that the TNT test results shown on figure 7 are consistently several degrees higher than the predicted angles. Experiments with planar shock waves on wedges show results similar to the TNT test results (6:592). The persistence of regular reflection past the predicted point is known as the Von Neumann paradox. Many theories have been advanced to explain the persistence, but none have gained widespread acceptance (61:180), (6:600-2).

In contrast to the TNT test results, the data from the nuclear tests does not show any particular pattern except that the triple point forms before the theory predicts. The precursor is believed to be the reason for this. The radiation from the weapon heats the air near the ground and changes the properties of that air. Thus the Mach stem may form earlier and rise faster in this region. When the precursor effect dies

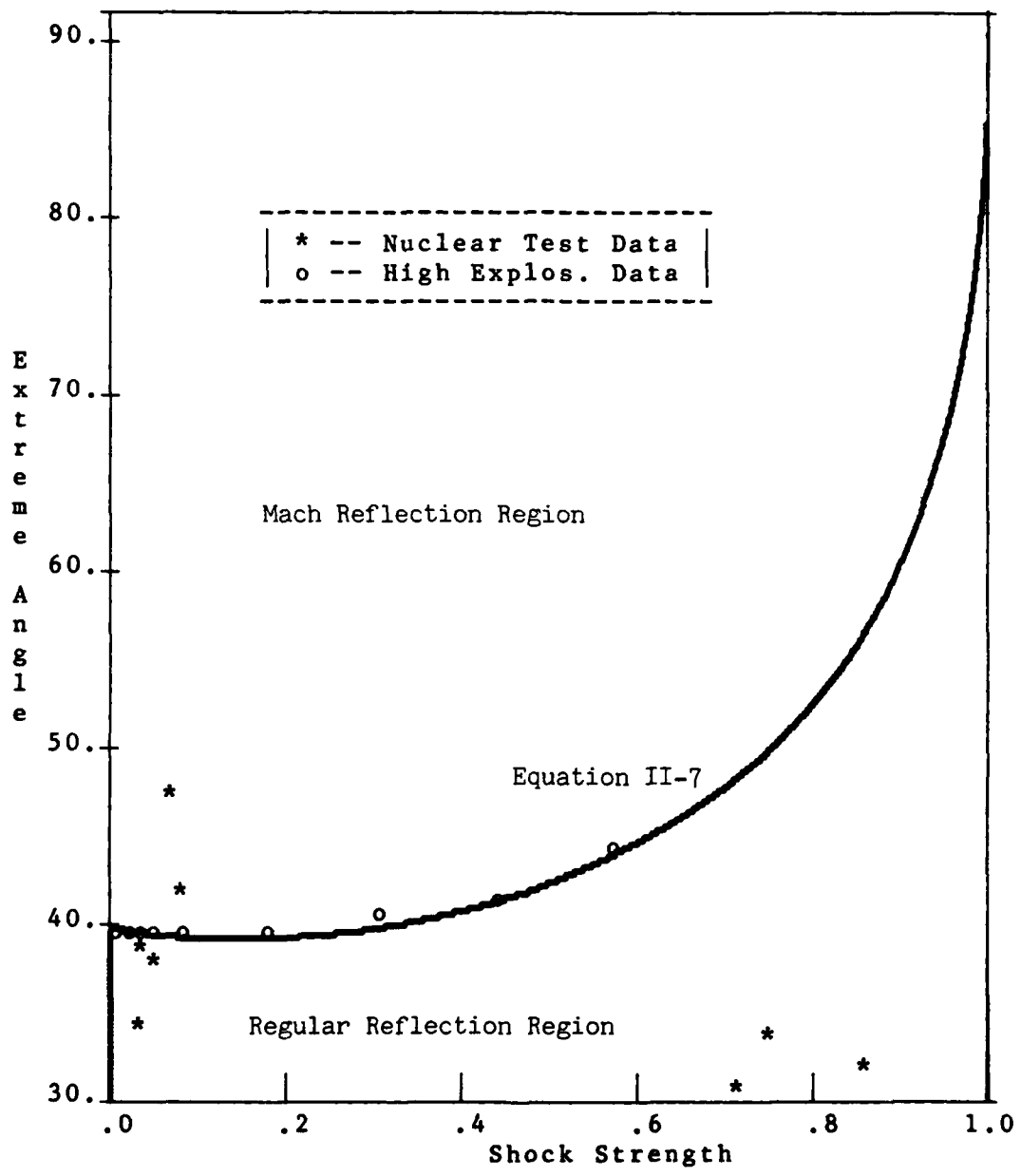


Fig. 7. Variation of Extreme Angle with Strength

out, the path of the triple point becomes very irregular. It has even been observed to decrease in height as the precursor died out and then increase again along a path closer to predictions based upon theory and HE experiments. Because of the amount of dust near the ground and the precursor effect, the actual origins of the triple points are not accurately known. Much of the test data gives conflicting results and thus many conflicting data points can be quoted from the literature. Shock photography does not give good results until the Mach stem has risen above the dust and ground clutter (which is generally a height of at least ten feet). For a scaled height of burst of 400 feet, the Mach stem may have traveled over 2500 feet by the time it gets to these heights. Thus backwards extrapolation to find the OTP is not very reliable (See also (45:195)).

Three Shock Theory.

Figure 8 is a diagram of the notation to be used in this discussion of three shock theory. There are four general regions to be considered in the analysis of the three shock configuration. Region 1 is the ambient air and region 2 is the shocked area between the incident and reflected waves. Regions 3 and 4 are the area behind the Mach shock. The air in region 3 has passed through both the incident and reflected shock while that in region 4 has passed through only the Mach shock. The configuration will be analyzed from the point of view of an observer traveling with the triple point. To the observer in the laboratory frame of reference, the triple point rises at a constant rate which can be expressed as the angle ψ . As stated before, the flows are self-similar. That is, the dimensions of the flow are a function of time only.

To an observer on the triple point, the ambient air is flowing towards him at a speed of $U_1 = U_s/\sin \phi_1$, where U_s is the incident shock velocity and ϕ_1 is the angle shown in figure 6. ϕ_1 is equal to $90 - \theta - \psi$. The velocity of this ambient air is parallel to the trace of the triple point. In describing the three shock configuration, twelve equations may be written. They are statements of conservation of mass, momentum and energy across each of the three shocks.

$$\rho_1 \tan \phi_1 = \rho_2 \tan(\phi_1 - \delta_1) \quad (\text{III-9})$$

$$\rho_1 U_1 \sin \phi_1 = \rho_2 U_2 \sin(\phi_1 + \delta_1) \quad (\text{III-10})$$

$$P_1 + \rho_1 U_1^2 \sin^2 \phi_1 = P_2 + \rho_2 U_2^2 \sin^2(\phi_1 - \delta_1) \quad (\text{III-11})$$

$$H_1 + \frac{1}{2} U_1^2 \sin^2 \phi_1 = H_2 + \frac{1}{2} U_2^2 \sin^2(\phi_1 - \delta_1) \quad (\text{III-12})$$

$$\rho_2 \tan \phi_2 = \rho_3 \tan(\phi_2 - \delta_2) \quad (\text{III-13})$$

$$\rho_2 U_2 \sin \phi_2 = \rho_3 U_3 \sin(\phi_2 - \delta_2) \quad (\text{III-14})$$

$$P_2 + \rho_2 U_2^2 \sin^2 \phi_2 = P_3 + \rho_3 U_3^2 \sin^2(\phi_2 - \delta_2) \quad (\text{III-15})$$

$$H_2 + \frac{1}{2} U_2^2 \sin^2 \phi_2 = H_3 + \frac{1}{2} U_3^2 \sin^2(\phi_2 - \delta_2) \quad (\text{III-16})$$

$$\rho_1 \tan \phi_3 = \rho_4 \tan(\phi_3 - \delta_3) \quad (\text{III-17})$$

$$\rho_1 U_1 \sin \phi_3 = \rho_4 U_4 \sin(\phi_3 - \delta_3) \quad (\text{III-18})$$

$$P_1 + \rho_1 U_1^2 \sin^2 \phi_3 = P_4 + \rho_4 U_4^2 \sin^2(\phi_3 - \delta_3) \quad (\text{III-19})$$

$$H_1 + \frac{1}{2} U_1^2 \sin^2 \phi_3 = H_4 + \frac{1}{2} U_4^2 \sin^2(\phi_3 - \delta_3) \quad (5:14) \quad (\text{III-20})$$

In addition to these general relations, several boundary conditions apply that are related to the existence of the slipstream. The slipstream is a surface that separates two regions of equal pressure and direction of flow. The two regions have different temperatures, entropy and density. This is because the air in region 3 has been shocked twice, by both the incident and reflected shocks, while the air in region 4 has

been shocked only once. Because of the equality of pressure across the slipstream, the boundary condition may be written:

$$P_4 = P_3 \quad (\text{III-21})$$

The direction of the flow along the slipstream must also be the same on both sides. This implies that the air passing through the Mach shock must be deflected through the same angle as the air passing through the other two shocks. Thus:

$$\delta_3 = \delta_1 + \delta_2 \quad (\text{III-22})$$

With the equation of state to relate the properties of enthalpy, temperature, pressure and density, the above 14 equations contain 18 variables ($P_1, P_2, P_3, P_4, U_1, U_2, U_3, \rho_1, \rho_2, \rho_3, \rho_4, T_1, T_2, T_3, T_4, \delta_1, \delta_2, \text{ and } \delta_3$ (5:15)). In setting up an experiment, the only initial conditions are $P_1, U_1, \text{ and } T_1$. The wedge angle is also known, but its use to define any of the other angles involves another variable, ψ . In contrast to Two-Shock theory, Three-Shock theory is indeterminate. In order to solve these equations, an additional assumption must be made. The most common is to set the angle ϕ_3 equal to $90-\psi$. This assumption is equivalent to assuming that the Mach stem is straight and perpendicular to the wedge. With this additional relation, the system may be solved, usually by some iterative method.

The above relations describe the shape and motion of the three-shock system only for the case of strong shocks. Figure 9 compares the predictions of two and three shock theory for the case of a weak and a strong shock. It should be noted that two shock theory is good for weak

shocks. The failure of three shock theory is often attributed to its failure to account for viscous and heat conduction effects (29:56), (15:345). While three shock theory does fail to account for these effects, it has never been shown that their inclusion will correct its deficiencies in the case of weak shocks.

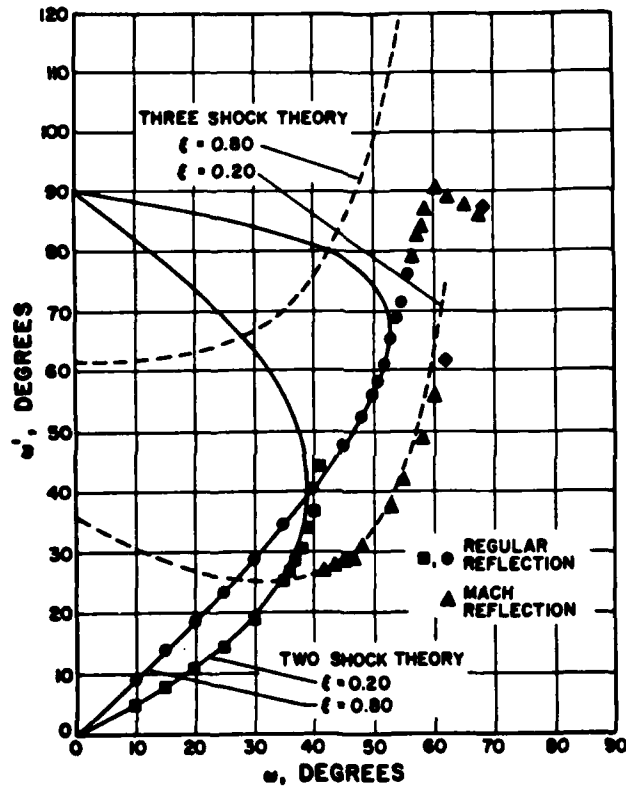


Figure 9. Comparison of Two and Three Shock Theory and Experiment
(29:57)

IV. Prediction of the Path of the Triple Point.

Prediction by Theory

In order to predict the path of the triple point for spherical shocks, one must be able to predict the value of ψ . ψ is the instantaneous trajectory angle of the triple point. In planar shocks, this angle is constant. In the case of spherical shocks, as the triple point rises, the angle of incidence changes continuously, and thus the angle at which the triple point is instantaneously rising changes accordingly. The path of the triple point is given by the following relation:

$$\text{Height of Triple Point} = \int_0^R \tan \psi \, dr \quad (\text{IV-1})$$

Thus the ability to trace the path of the triple point is based upon the ability to accurately predict the angle ψ for all cases under consideration.

In order to predict this angle, three different cases had to be investigated. Planar shock theory as outlined in the previous section will give good solutions only for the case of strong shocks. Experimental data is used when the incident shock Mach number falls below 2. However, when the triple point rises to a height greater than the height of burst, there is no theory to predict the results nor is there any experimental data. This is caused by configuration of the shocks in

which the incident shock does not precede the system. In this region the author developed a model to predict the value of ψ .

Strong Shock Solution

The solution for the strong shock case is based upon a method advanced by Mirels (44:b1-3). The original method was worked out for the case of infinitely strong shocks only. This derivation has removed this assumption and can accurately predict the angle ψ for incident Mach wave shock numbers as low as 2.

Six basic relations are required to solve the problem. The notation used is the same as that used for developing the three shock theory and can be seen in figure 6. The first of these relations describes an angle λ such that: (44:b2)

$$\lambda = \alpha - \beta - \theta \quad (\text{IV-2})$$

Once again the oblique shock relations are used to find the ratios of pressure and density across the incident shock. The frame of reference is the one in which the triple point is stationary. The density ratio is denoted as K1 and the pressure ratio is denoted as K2 for later convenience and simplification of the final relations. Thus the pressure and density ratios can be found from:

$$\frac{\rho_2}{\rho_1} = \frac{(\gamma+1)M_1^2 \cos^2(\theta + \psi)}{2 + (\gamma-1)M_1^2 \cos^2(\theta + \psi)} = K1 \quad (\text{IV-3})$$

$$\frac{P_2}{P_1} = \frac{2\gamma}{\gamma+1} M_1^2 \cos^2(\theta + \psi) - \frac{\gamma-1}{\gamma+1} = K2 \quad (\text{IV-4})$$

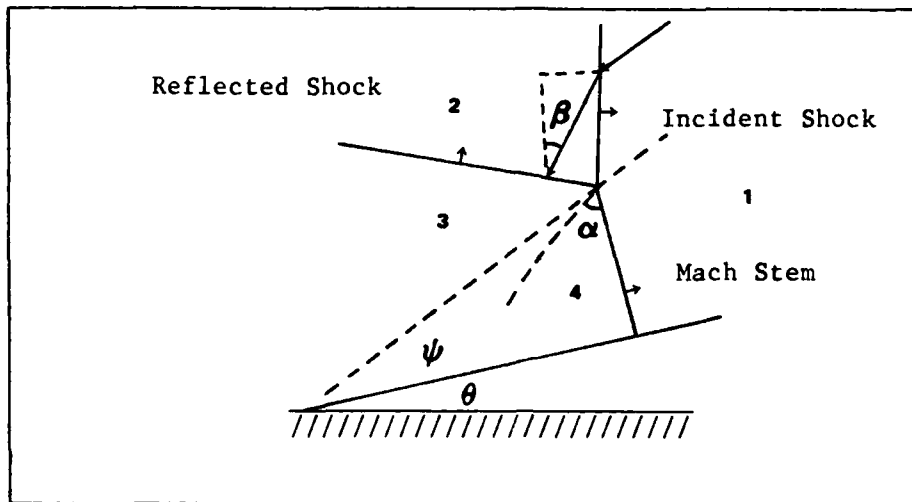


Figure 10. Regions and angles for Strong Shock Relations.

The next relation is the ratio of the airflow in region 2 that is tangent to the direction of motion to that which is perpendicular to the direction of motion. The component of velocity of the incident flow that is parallel to the shock front is not altered by the passage of the air through the front. Thus the tangential velocity in region 1 is the same as the tangential velocity in region 2. The velocity component that is perpendicular to the shock front is decreased in magnitude by an amount that can be measured by the density ratio which has been designated as K_1 . This ratio of airflow in region 2 defines the angle β in the following manner.

$$\frac{V_{t_2}}{V_{n_2}} = \cot \beta = \frac{V_{n_1}}{V_{n_2}} \frac{V_{t_1}}{V_{n_1}} = \frac{\rho_2 \sin(\theta + \psi)}{\rho_1 \cos(\theta + \psi)} = K_1 \tan(\theta + \psi) \quad (\text{IV-5})$$

Similarly in region 4 the angle α defines the angle of the flow as does β in region 2. α is also the angle between the slipstream and the

Mach shock. In front of this region, the air is moving into the Mach stem at an angle of ψ . Thus the ratios of densities and pressures are defined by the following relations and designated K3 and K4.

$$\frac{\rho_4}{\rho_1} = \frac{(\gamma+1)M_1^2 \cos^2(\psi)}{2+(\gamma-1)M_1^2 \cos^2(\psi)} = K3 \quad (\text{IV-6})$$

$$\frac{P_4}{P_1} = \frac{2\gamma M_1^2 \cos^2(\psi) - \gamma - 1}{(\gamma+1)\cos^2(\theta + \psi)} \frac{\gamma - 1}{\gamma + 1} = K4 \quad (\text{IV-7})$$

Notice that this formula assumes that the Mach stem travels at the same velocity as the incident shock. To an observer on the triple point who is assumed to be stationary, the ambient air appears to be moving towards him with constant speed and direction. This velocity is defined by the velocity of the incident shock. Since the shock configuration is assumed to be self-similar, the air must approach the Mach stem at the same speed, but with a different direction than the air approaching the incident shock. By assuming that the angle between the Mach shock and the incoming air is ψ , one is assuming that the Mach shock is perpendicular to the wall and remains that way.

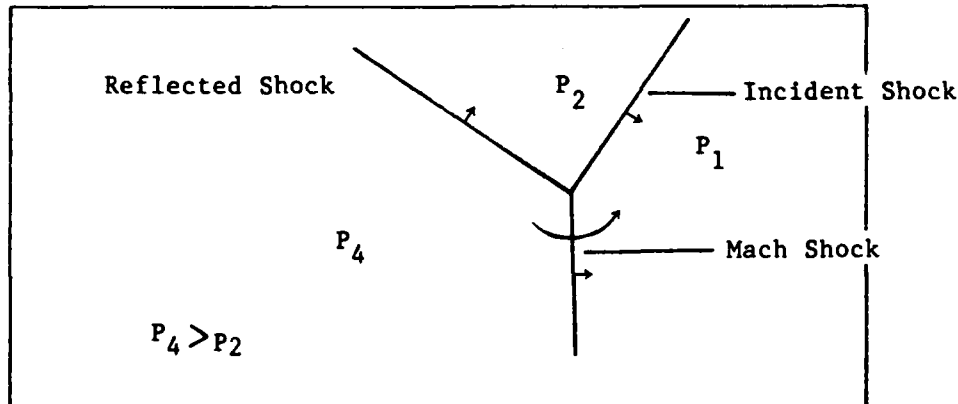


Figure 11. Shock Configuration in Frame of Triple Point Stationary

Figure 11 is a simple diagram of the shock configuration from the point of view of an observer riding on the triple point. This observer sees three stationary shocks. This observer also sees that the overpressure in region 4 is greater than that in region 2. Because of this difference in overpressure, he would expect that the Mach shock would rotate forward.

Laboratory observations have shown that the Mach stem can be considerably curved and tends to bulge forward. This implies that the velocity of the Mach stem is greater than in the incident shock in the direction parallel to the wedge surface. Thus to the observer on the triple point, the Mach stem should toe out and appear to rotate or develop curvature. Both effects have been observed. Sternberg studied the curvature in Mach shocks and proposed that as a reason for the apparent lack of agreement between theory and experiment (61:182). The towing out phenomenon can be seen clearly in many photographs of Mach stems (39:fig 7-11,k,1) (17:b43).

The actual angle of incidence of the ambient air on the Mach stem is more correctly described by an angle $\psi - \sigma$ where σ represents an amount of rotation or curvature. However, this destroys the self-similarity assumption made earlier. The airflows will depend on the degree of rotation about the triple point and which changes with time and distance traveled. The introduction of another variable requires another condition for solution of the system. This causes the same problem as in the solution to the three shock system before. There will always be too many variables and too few conditions unless some assumption is made. It is useful to recognize at this point that the Mach stem can be expected

to toe out and not remain vertical to the ground in the region of the triple point.

From the frame of reference of an observer located at the base of the Mach stem (point E in figure 8), the flow of air must be parallel to the wall at all points. If the shock was deflected towards the ground, a reflected shock would be generated at some point to the rear of the Mach shock. Similarly if the flow were diverted upwards, it would cause a low pressure area to be generated to the rear of the Mach shock. The requirement for flow parallel to the wall requires that the Mach stem be perpendicular to the wall in the region near point E. Thus regardless of the angle of the Mach stem in the vicinity of the triple point, the Mach stem must intersect the wall surface at a 90 degree angle. Given the fact that the Mach stem rotates about the triple point, the Mach stem must have a curvature that changes with time.

By the same logic as that which defined the angle β in equation IV-5, α may be defined with the following relation:

$$\cot \alpha = K_3 \tan \psi \quad (\text{IV-8})$$

The strength of the reflected shock is defined as $\xi = P_2/P_3$. Because the pressure across the slipstream is constant, $P_3 = P_4$. Thus the strength of the reflected wave can be expressed in terms of the pressures in regions 2 and 4 which can be found from the oblique shock relations.

$$\xi = \frac{P_3}{P_2} = \frac{P_4}{P_2} = \frac{P_4/P_1}{P_2/P_1} = \frac{K_4}{K_2} \quad (\text{IV-9})$$

The ratio of the velocities of the air in regions 1 and 2 are given by Mirels as (44:bl):

$$\frac{V_2}{V_1} = \left(\frac{K_2}{K_1}\right)^2 M_2 = \frac{1}{K_1 \sin \beta} \quad (\text{IV-10})$$

Mirels also gives a relation developed using the method of characteristics for the flow over wedges of half-angle λ in free flowing air. This equation can be used to unite the preceding relations.

$$\tan^2 \lambda = \left\{ \frac{C_1 C_2 M_2^2 - 1}{1 + C_1 \xi} \right\} \cdot \left\{ \frac{\xi + 1}{M_2^2 - \gamma + 1} \right\}^2 \quad (\text{IV-11})$$

$$\text{Where } C_1 = (\gamma + 1)/(\gamma - 1)$$

$$C_2 = 2\gamma/(\gamma + 1)$$

Using the above relations, equation IV-11 can be expressed as a function of the variables θ and ψ only. Because of the complexity of the relation, it has not been possible to separate the equation to find ψ directly. Even if it could be done, the parameters K_1 through K_4 are also functions of the angle ψ . Hence some iterative method of solution must be used to find this angle. The relation expressed in terms of θ and ψ is as follows:

$$\left\{ \frac{K_1 \cot \psi + K_1 K_3 \tan \theta + \cot(\theta + \psi) [\cot \psi \tan \theta + K_3]}{K_1 K_3 + K_1 \cot \psi \tan \theta + \cot(\theta + \psi) [K_3 \tan \theta - \cot \psi]} \right\}^2$$

$$= \left\{ \frac{C_1 C_2 (1 + K_1^2 \tan^2(\theta + \psi)) - 1}{(1 + C_1 K_2 / K_4) K_1 K_2} - 1 \right\} \cdot \left\{ \frac{K_1 K_2 (K_2 / K_4 - 1)}{[1 + K_1^2 \tan^2(\theta + \psi)] - K_2 / K_4 + 1} \right\}^2$$

(IV-12)

The above relation is used to find the angle ψ for the situation of a

strong shock, $\xi < .15$. For weaker shocks ($\xi > .15$), the theory predicts a much higher angle ψ than is experimentally found and predicts that regular reflection terminates at an earlier angle of incidence than experiments show. Thus some other means of predicting this angle is required in the region of weak shocks.

Use of Experimental Data.

Experimental data was used by this author to derive a set of curves which would be used to predict the angle ψ given an incident shock strength and angle of incidence. The data used was a set of fitted curves for ψ given by Harlow (29:56) and supplemented by a series of experiments done at the University of Toronto (5:table 5), (17:bl) in air and nitrogen. Curves were fitted to the following shock strengths, .15, .30, .40, .50, .60, .70, .80, and .90. Shocks with strengths between the fitted values are found by linear interpolation.

The set of curves was checked against the actual data for accuracy and found to predict the value of ψ to within ten percent. The comparison in accuracy is particularly striking with respect to the prediction of the onset of Mach reflection. For example, the computational technique presented above predicts Mach reflection to begin at a Mach number of about 1.325 for a wedge angle of 40 degrees. This model predicts the onset at about 1.175. The experimental value is a Mach number of approximately 1.2. At higher Mach numbers the two predictions merge to the same answer.

The set of curves used here could be substantially improved if additional detailed data was available for weak incident shocks. The

Toronto experiments covered wedge angles of two degrees to 50 degrees and Mach numbers ranging from 1.6 to 6.9. Referring to figure 19, it can be seen that at low Mach numbers, small errors can make much larger errors in the value of ψ . Because of the way the data is used, more detailed information from experiments at low Mach numbers and small wedge angles would enhance the predictions considerably.

Solution for Heights Greater than Height of Burst.

When the height of the triple point reaches the height of burst, the shocks assume a new configuration (see figure 12). This configuration is not reproducible in the laboratory with planar shocks on wedges. The Mach shock theory described before does not work well for angles of incidence greater than 85 degrees (40:3,8). The equations do not give meaningful answers for shocks with angles of incidence greater than 90 degrees either. Thus a new method of examining the problem was developed by this author.

Generally, certain assumptions are made to make the problem solvable. Both the incident and the reflected shocks are assumed to be spherical in shape. The inhomogeneity of the atmosphere and its effect on the shape of the incident shock are ignored. The large variations in pressure and density that occur in the region behind the incident shock may cause large deviations from spherical symmetry in the reflected shock, especially near ground zero. However, the triple point reaches the height of burst at a ground distance greater than five to six times the height of burst. By this time, the incident shock has lost much of its strength and is barely sonic for scaled heights of burst greater than 200

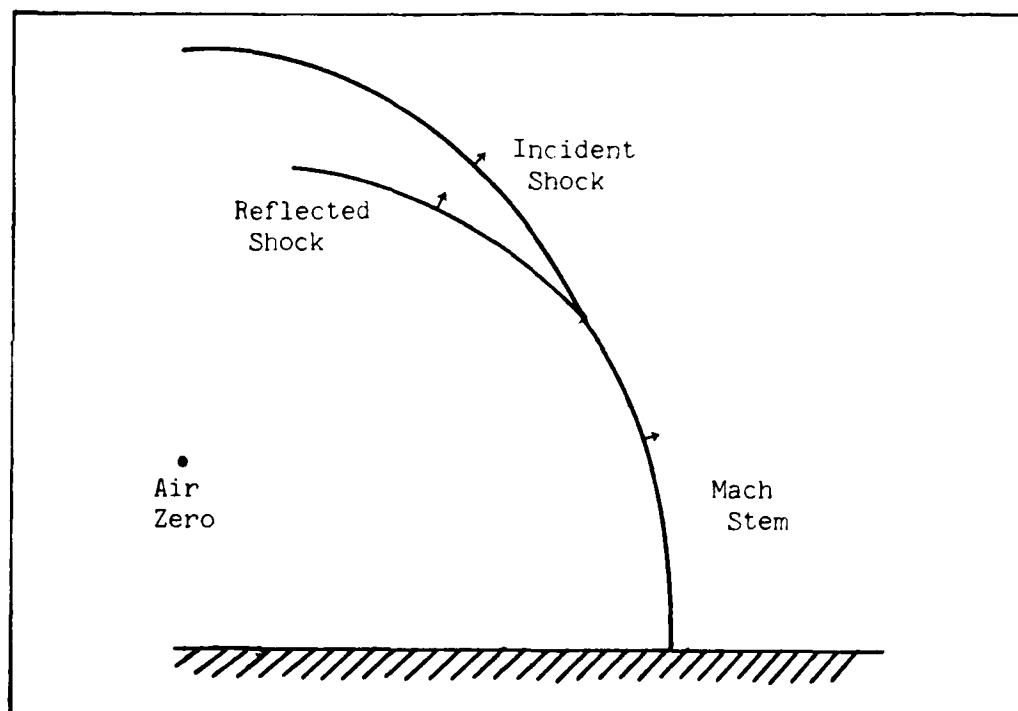


Figure 12. Shock Configuration at Late Times

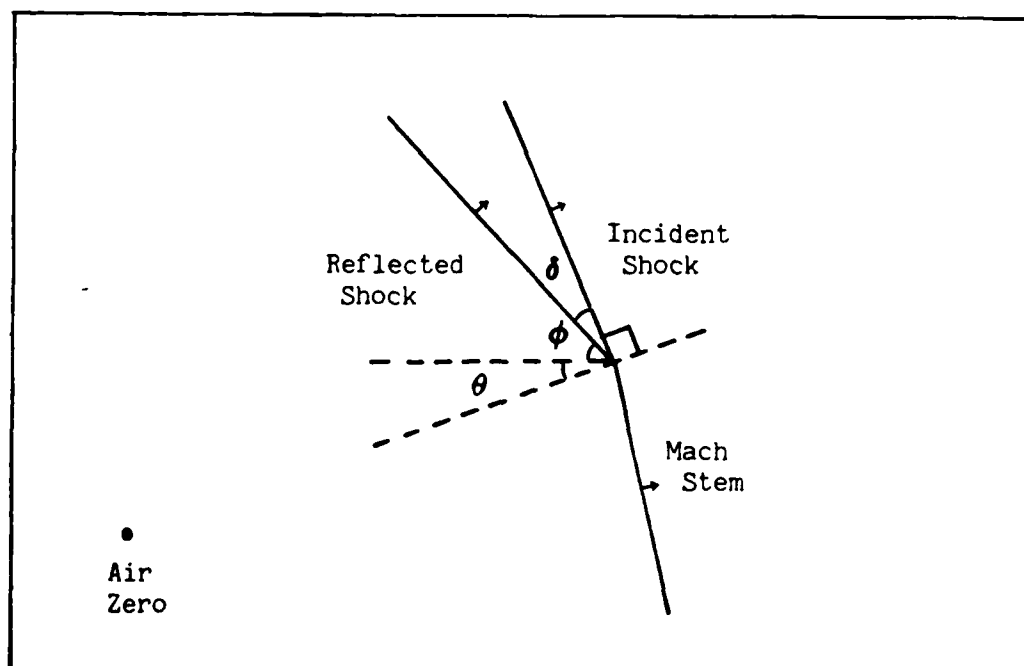


Figure 13. Planar Approximation

feet. Because of this fact, the shock can be approximated as spherical and an acoustic reflection approximation made. For weak shocks, the angle of reflection is equal to the angle of incidence. Similarly, the overpressure in the reflected shock is equal to the incident shock. From the acoustic approximation, the shape and strength of the reflected shock can be found from an 'image burst' fired at a point one height of burst below the surface of the earth at ground zero. The overpressure of the reflected shock is assumed to be the same as a shock traveling in free air from the image burst. Simple geometrical relations may then be used to find the angle of incidence and the angle between the two shocks. Once these angles are known, the shocks are treated as planar shocks for that instant in time, and the angle ψ calculated.

The movement of the intersection of the two planar shocks is illustrated in figure 13. The velocities of the incident and reflected shocks are designated V_1 and V_2 respectively. The x and y directions are parallel and perpendicular to the plane of the earth's surface. The amount of movement in each of these directions during an infinitesimal time dt can be found from the following relations:

$$dx = \frac{\cos \phi}{\sin \delta} V_1 dt - \frac{\cos(\phi + \delta)}{\sin \delta} V_2 dt \quad (IV-13)$$

$$dy = \frac{\sin(\phi + \delta)}{\sin \delta} V_2 dt - \frac{\sin \phi}{\sin \delta} V_1 dt \quad (IV-14)$$

The velocity of each shock can be measured easily in terms of the Mach number of each shock which in turn can be found from the overpressure. However, the reflected shock travels faster in the air behind the

incident shock than it could in ambient air. Thus the true velocity of the reflected shock is not given by the image burst. The difference in velocity can be estimated from the ratio of the sound speeds in the shocked and unshocked air. Using the Rankine-Hugoniot relations, the following relationship was found:

$$\left(\frac{S_2}{S_1}\right)^2 = \frac{(P_o+dP)(7P_o+dP)}{P_o(7P_o+6dP)} = f^2 \quad (\text{IV-15})$$

Where: P_o = ambient atmospheric pressure

dP = overpressure in the incident shock

S_2 = sound speed in the shocked air

S_1 = sound speed in the ambient atmosphere

It should be noted that the speed of sound in the shocked air may vary greatly from area to area. The ratio above is an attempt to quantify the velocity of the reflected shock in the area immediately behind the incident shock. Using the above relation and the fact that $\tan \psi = dy/dx$, a relationship may be written:

$$\psi = \text{atn} \left[\frac{M_2 f \sin(\phi + \delta) - M_1 \sin \phi}{M_1 \cos \phi - M_2 f \cos(\phi + \delta)} \right] \quad (\text{IV-16})$$

Where: $(\phi + \delta) = 180$ - angle of incidence

$\phi = 90$ - $\text{atn}[(\text{HTP} + \text{HOB})/\text{ground distance}]$

f = ratio of sound speeds

The relations immediately preceding may be used whenever the height of the triple point is greater than the height of burst. The angles generated by this method compare favorably to the angles found by analysis of the triple point path data in the Reflect-4 computer codes

(58:147-173). Reflect-4 is a two-dimensional hydrodynamics code for the analysis of Mach reflection. The angles found by the method above are consistently less than the reflect code would indicate by about 20 percent. This would seem to indicate that the reflected shock wave travels faster than the estimate based upon the ratio of sound speeds.

In evaluating the above set of equations, there are two limiting cases that they must converge to. For low heights of burst, the triple points on each side of the burst will rise very quickly and meet above the burst, creating a shock system similar to a contact surface burst. For very high heights of burst and at long distances, the reflected shock will be very weak in relation to the incident shock. Thus the angle ψ will converge to some value and not change significantly. The method described here does predict that for low heights of burst, the triple points will arch back and meet above the burst. However, in the case of high heights of burst and long distances, the equations predict that the angle ψ will continue to grow in magnitude. Thus the method described above should be used with care since it appears not to be universally valid for all situations.

Comparison to Nuclear Explosions

The computer program in Appendix F utilizes the methods in this chapter to trace the trajectory of the triple point in space. The equations given are used in each of the three regions to predict the angle ψ . This angle is then used in equation IV-1 and integrated using Simpson's rule. Two scaled heights of burst were selected for comparison. Teapot number 4 and number 12 were two shots with a 135 foot scaled HOB. The path of the triple point was determined in detail for

these two shots and present a good example of the degree of correlation between any estimates and an actual detonation. The second comparison is made for a 700 foot scaled HOB using the Reflect-4 Code determinations. Reflect-4 is a two-dimensional hydrodynamic code used for Mach stem studies by the Kaman Avidyne Corporation. The comparison with this prediction will enable a comparison with current state of the art in shock modeling. In each case, the prediction based upon Potocki's curve-fits to EM-1 will be used to show how well current practice relates to the same examples. The curves in EM-1 are the basis for most of today's predictions of the triple point trajectory. These curves are directly traceable to the work of Hesse and Kelso in 1955 (35:11,22,23).

Figure 14 shows the comparison between the two Teapot detonations and the program predictions for a 135 foot scaled height of burst. The prediction made by the program is too low at early times and too high at much later times. To some extent, the rapid rise of the triple point from the Teapot detonations is due to precursor activity. The Mach stem formed much earlier than predicted and rose much faster. This may account for some of the discrepancy. There is a large percent difference in triple point height just between the asphalt and soil surfaces in the Teapot 12 tests. The water surface on that test would correspond to the most ideal surface expected. The calculations are much lower than even this surface.

At a 700 foot scaled height of burst the prediction does much better (Figure 15). In general, the prediction is better than Potocki's prediction. The change in slope of the prediction at the altitude of the burst is caused by the change in routines from experimental data to the

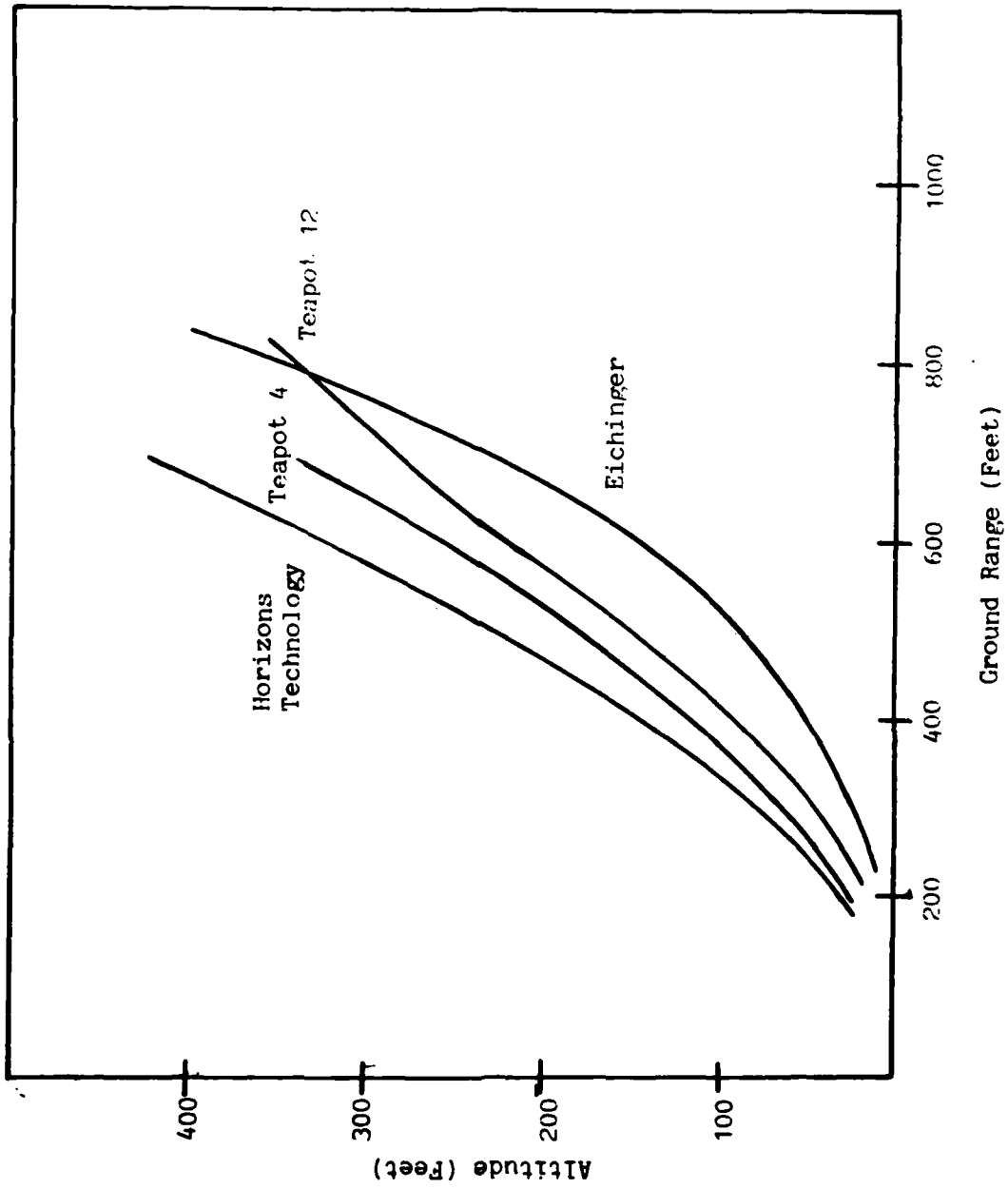


Figure 14. Triple Point Trajectory Comparison 135' SHOB

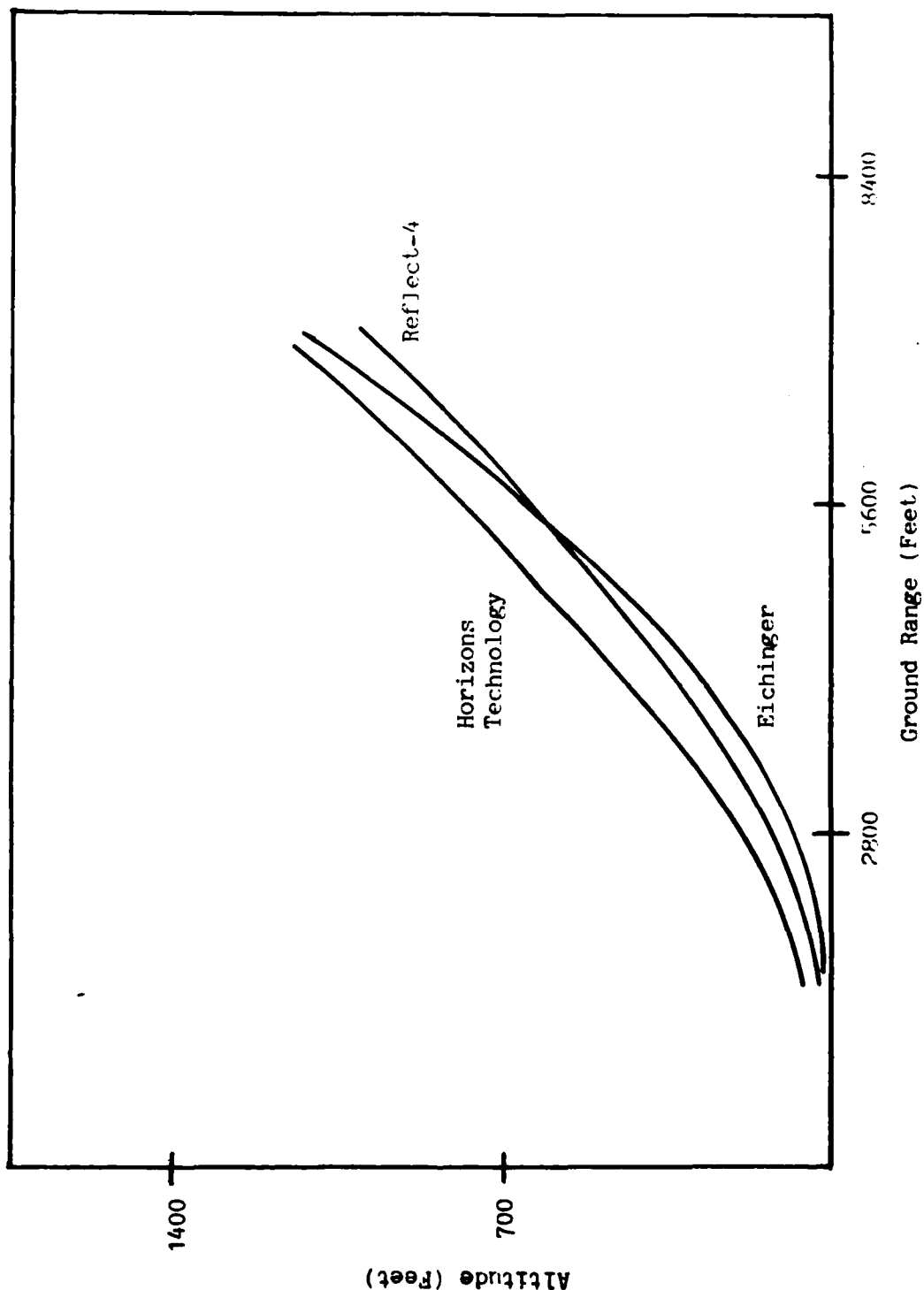


Figure 15. Triple Point Trajectory Comparison 700' SHOB

expression used to find ψ at altitudes above the triple point. The experimental data used is weak in this area and needs to be improved.

The results for the 135 foot scaled height of burst are indicative of the problem of prediction of the triple point trajectory. For the same burst, but for different ground types, the path was very different. There is also the large difference between Teapot 4 and Teapot 12. They were fired in similar atmospheric conditions, over the same type of soil, and in the same season of the year. The actual yield of the weapon and height of burst were different and caused a large difference in the triple point heights at the same scaled range. It seems reasonable to conclude that errors on the order of ten to twenty percent in the height of the triple point are reasonable at the level of prediction ability available today. The addition of more physics into the prediction, and taking into account the precursor heating of the air, the change in air density with temperature and altitude may enable a better prediction of the path. However, the addition of these effects means that the prediction will take considerably more time to calculate and will be device and location dependent. These factors are not desirable for many uses.

V. Empirical Results for Shape, T_a , and Overpressure.

To the military targeteer, the effects that must be known in order to predict the damage to aircraft and missiles in the path of the Mach stem include the shape or orientation of the shock wave, the overpressure, the dynamic pressure, and the time of arrival. These effects when combined with the type and orientation of the aircraft allow determination of the probability of survival. Presently the Mach stem is assumed to be vertical at all points above the ground. The time of arrival and overpressure may be approximated by the time of arrival and overpressure on the ground. The overpressure at altitude is scaled using Sachs scaling. Current shock theory is not capable of predicting any of these effects at any point for any geometry.

Shape and Orientation of the Shock Wave.

The examination of photographs of above-ground nuclear bursts as well as data from hydrodynamic calculations such as Reflect-4 clearly demonstrate that the assumption of a vertical Mach shock is wrong. Examination of the data shows that there are in fact three distinct shapes to the Mach stem (See figure 16). At early times, the triple point leads the base of the Mach stem by as much as ten percent of the ground range. For low heights of burst such as 200 scaled feet, the triple point may lead as much as fifteen to seventeen percent (59:30,150). During this period, the Mach shock is concave inward. As the triple point approaches the height of burst, the base of the Mach

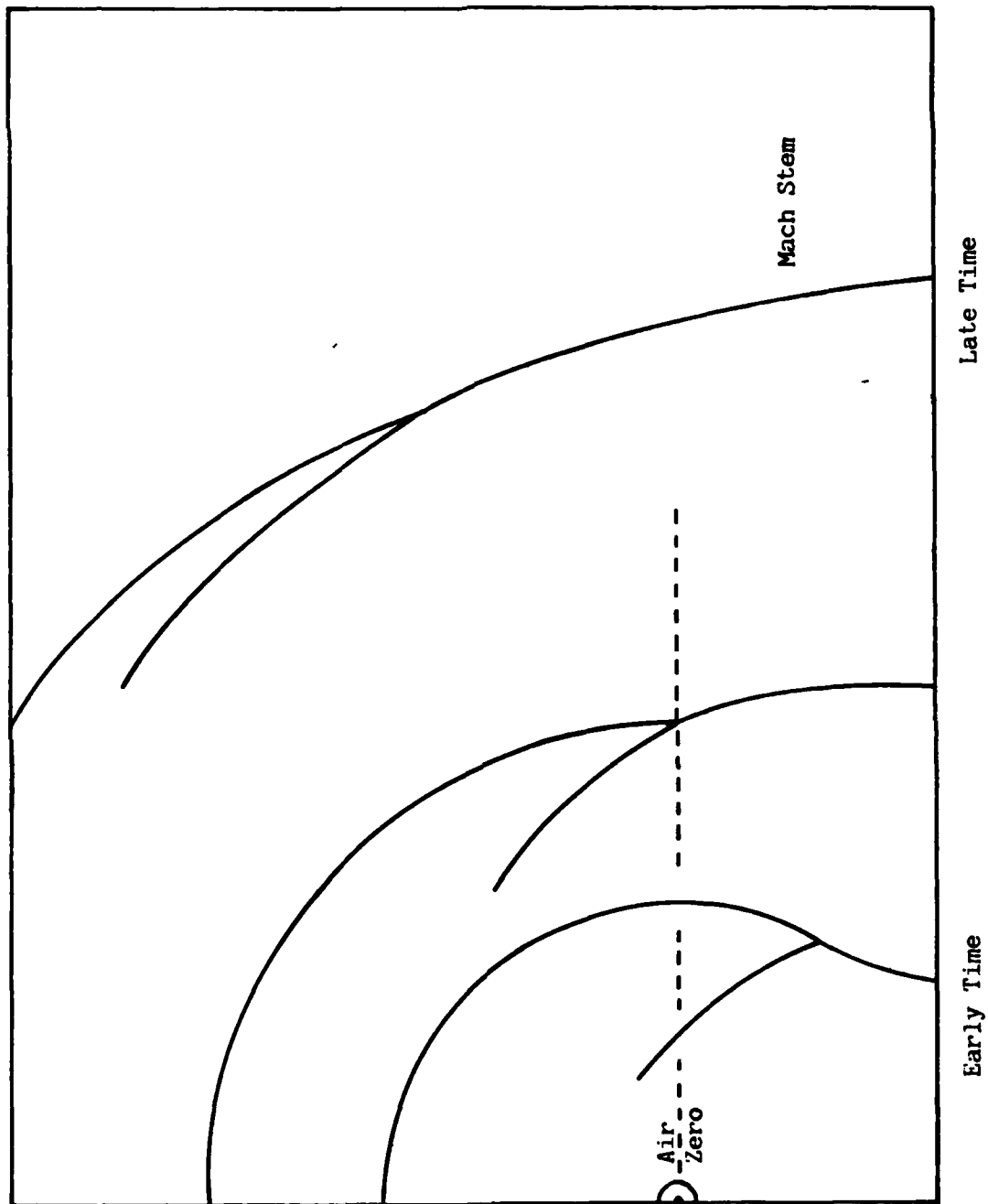


Figure 16. Variation of Mach Stem Shapes With Time

shock catches up and the Mach stem is approximately vertical. As the height of the triple point continues to rise, the base of the Mach stem begins to lead the triple point. As time goes on, the shape of the entire shock system of the incident shock and Mach shock, approaches a hemispherical shape centered at ground zero. Because of the increase in speed of the shock at low heights of bursts due to the layer of heated air near the ground, this hemispherical shape can be introduced by the time the Mach shock is 50 feet high (45:166,201). In other words, the presence of precursor conditions may enhance the tendency towards the hemispheric shape.

The airflow in the vicinity of the triple point requires that the mach stem lead the incident shock when the triple point is above the height of burst. In this case, the incoming air is deflected upward by the incident shock (See figure 17). The upward deflection is caused by the angle of intersection between the incoming air and the shock (Designated ϕ in figure 17). Where before the angle was acute, the angle in the new configuration is obtuse. The reflected shock also has an obtuse intersection angle and deflects the flow of air upward. If the mach shock is to deflect the air through the same angle as the other two shocks (i. e. $\delta_1 = \delta_2$), it must lead the incident shock. If the shock was vertical, the air would be deflected down by the mach shock, causing the airflow behind the triple point to be discontinuous. This discontinuity does not occur. As the three shocks lose their energy, the reflected shock becomes weakest first. When it is very weak, the deflection angle of the air due to it will become negligible. When that happens, the deflection caused by the incident shock must equal the

deflection of the mach shock. At this time the tangents of the two shocks must converge.

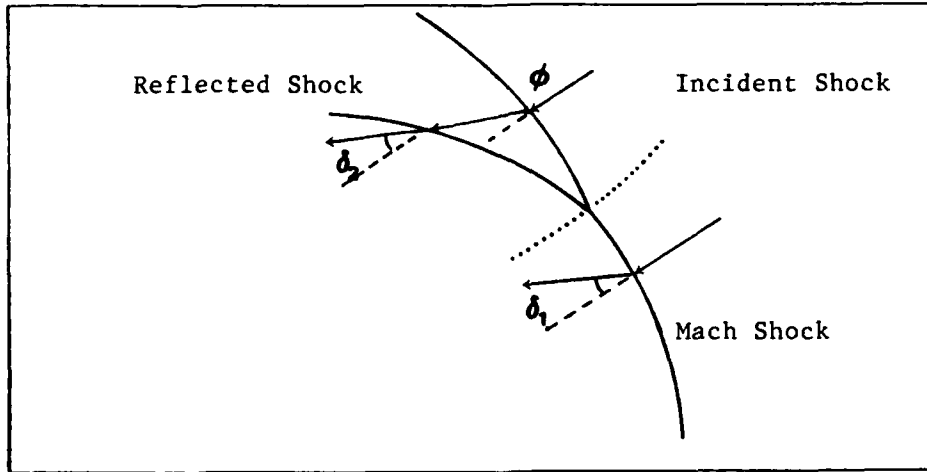


Figure 17. Airflows Near Triple Point When HTP is Greater than HOB

Since damage due to overpressure for aircraft occurs in the 1 to 20 psi. overpressure range, the region of most interest is this distant region. The equations given here are valid when the triple point is higher than the height of burst. The effective radius of the Mach stem at these overpressures is given in table 1.

Scaled HOB (feet)	Scaled Ground Range (feet)	Scaled Effective Radius (feet)	Ratio
200	705	728	1.1
400	4,982	9,878	1.98
700	5,614	15,833	2.77

Data from analysis of reference 59.

Table 1. Effective Radius of Mach Stem

The radius of the Mach stem decreases more slowly at higher scaled

heights of burst because it grows in height many times more slowly. The lower the height of burst, the sooner it resembles a contact surface burst to a distant observer. In fact, the Reflect codes predict that for a 200 foot scaled height of burst, the triple point will continue to rise after surpassing the height of burst elevation, but will decrease in ground range. Then the entire shock front rapidly becomes reinforced so that within one-half second of the triple point passing the height of burst, the Mach stems meet at the apex of the shock front (59:151). The effective radius of the Mach stem at large distances from ground zero may be approximated by the following empirical formula, which is a curve fit to the data in Table 1.

$$\text{Eff. Radius} = R_e = (.0000573\text{SHOB}^2 + .317\text{SHOB} + .574)(\text{Gnd. Range}) \quad (\text{V-1})$$

Where SHOB is Scaled HOB, measured in hundreds of feet.

Once the radius is known, the orientation of the Mach stem can be found. From this, the direction of the impulse imparted by the shock front with respect to the ground may be calculated. This direction is also the direction of the 'gust' that is used in the calculation of the wing loading. τ as given in the following equation is the direction normal to the shock surface.

$$\tau = \arctan\left(\frac{\text{Height of Target}}{\text{Effective Radius}}\right) \quad (\text{V-2})$$

Time of Arrival.

In attempting to find a relation that predicts the time of arrival, two basic relations were used. Both Horizons Technology (51:82) and Brode (8:15) give general relations for time of arrival in free air. The

Horizons Technology equation is essentially a curve fit to the one kiloton standard. To properly scale back to the desired case, detailed knowledge of the temperature and pressure of the target is required. Even with this knowledge for the original bursts, this equation failed to predict the actual time of arrival as well as the equation given by Brode (See table 2). The best fit found to predict the actual times of arrival is given by Brode: (8:15)

$$T_a = \frac{(.54291 - 21.185R + 361.81R^2 + 2383R^3)W^{1/3}}{(1 + 2.04797R + 2.68717R^2)} \text{ msec} \quad (V-3)$$

Where: R = Slant range to target (kilofeet) scaled by the yield and pressure on the ground.

W = Yield (kilotons)

T_a = Time of arrival (milliseconds)

This formula is accurate to within 7.7 percent of the actual values. Since the original slant ranges are known to within eleven percent, greater accuracy cannot be expected. In all cases but one, the formula predicts a slightly earlier time of arrival than is observed. The sole exception is the Ivy King test in which the actual time of arrival is consistently earlier than predicted. This burst differed from the others in that it was 550 Kt. and the others were 43 Kt. or less. The Ivy King test also differs from the other tests in that it appeared to have a much greater blast efficiency than previous tests. The free air and Mach stem overpressures were much greater than expected. The greater overpressure

would cause a decrease in time of arrival. Because cannister data is available for only one high yield weapon, it is not possible to tell if the Ivy King data is a device peculiar effect or to be expected of all high yield weapons.

Author	Yield	Min Error	Max Error	Ave Error
Brode	W	.22 %	7.69%	4.67 %
Brode	2W	.377%	14.3 %	8.53 %
Horiz Tech	W	.23 %	34.5 %	13.58 %
Horiz Tech	2W	1.3 %	33.5 %	11.16 %

Table 2. Comparison of Time of Arrival Equations for Mach Stem Data

The Mach shock seems to propagate at approximately the same speed as a free air shock at long distances. As shown earlier, at long distances the Mach shock assumes the hemispherical shape of the incident shock. Thus the entire shock system appears to a far observer to have a hemispherical shape. Under such conditions, the time of arrival of the Mach shock would seem to be the same as a free air shock at the same slant range. The equation given is valid then for arrival times greater than three seconds or when the height of the triple point is much greater than the height of burst.

Overpressures.

There are only two points in the Mach stem at which the overpressure may be estimated with any degree of certainty. These are the overpressure at the base of the Mach stem and the overpressure just below

the triple point. The overpressure at the base of the Mach stem is known from ground measurements made during the above ground nuclear tests. The overpressure may also be estimated by semi-empirical methods based upon the free air overpressure at equal ranges with considerable accuracy (8:14-27). However, in almost all cases, the overpressure measurements were made at real ground ranges of less than 5000 feet. The height of burst curves in EM-1 are accepted as the standard for the estimation of the ground overpressure. They also are limited to a scaled ground range of 4000 feet. Mathematical curve fits made from this set of curves may be used to extend the predictions with an accuracy of fifteen percent (See for example (52:42)). At the triple point, the overpressure may be found from equation IV-7. Since the Mach stem is not vertical, the true angle of incidence is not $90-\psi$, but some angle $90-\psi-\sigma$, where σ is the Mach stem's deviation from vertical. Thus for any given instant in time, one may find the value of the overpressure just below the triple point if he knows rate of rise of the triple point and the amount of deviation from vertical in the Mach stem.

However, the military planner needs to know the variation in pressure with height. The fact that the Mach stem changes curvature in itself is an indication that there is a pressure distribution along the Mach front. Analytical theory that would predict the physical characteristics of the Mach shock is nearly nonexistent in planar shock theory and completely nonexistent in the case of spherical shocks. In 1951 Fletcher, Bleakney, and Taub reviewed three theories that purported to describe conditions within planar shocks (26:271). Each of these theories was valid only in the region of vanishingly weak shocks and angles of incidence of nearly

90 degrees. Since that time, there have been no significant improvements. The most promising of the theories was one by Bargmann who predicted that the pressure in the Mach stem decreases monotonically with increasing vertical height along the shock and specified the shape of the pressure contours behind the Mach stem (4:43). The characteristic shape of these contours has been experimentally verified and taken as evidence for his theory. Apart from the expectation of a pressure variation with altitude, this theory is of little use over the wide range of shock strengths and angles of incidence to be found in a nuclear detonation.

During the atmospheric nuclear testing in the 1950s, cannisters occasionally were dropped to measure overpressures at altitude. Later, more sophisticated photographic techniques were used to measure free air shock velocities and overpressures. A total of 40 unclassified cannister measurements were made in the Mach region. Two more measurements are still classified. When the measurements were compared to the standard method of prediction, the measurements differed from the predictions in a consistent manner. Figure 18 is a plot of the actual data in terms of the fractional distance of the gage height up the Mach stem versus the measured overpressure divided by the predicted overpressure. The predicted overpressure was found by using the equations given by Horizons Technology (51:74-5). The height of burst in each case was scaled using the designated yield and ambient air pressure on the surface. The equations gave the overpressure on the ground for the 1 kiloton reference case. This pressure was then scaled to the altitude of the particular measurement using Sach's scaling. The ambient air pressures on the ground and at altitude are known in all cases from radiosonde readings

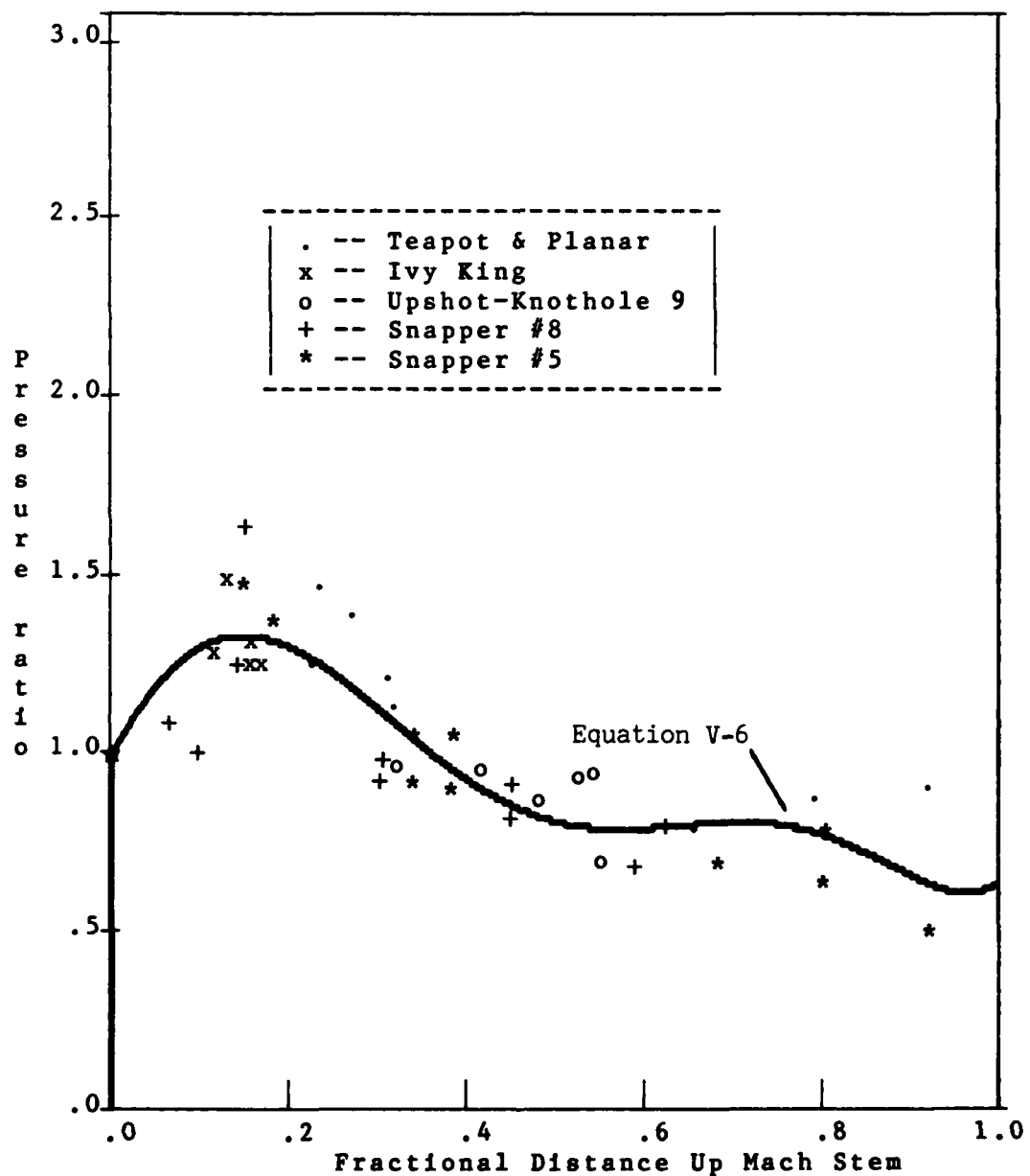


fig. 18 Variation of Pressure up the Mach Stem

before the tests. If the data agreed with the predictions, it would follow the line $y=1$. However, at heights of about 20 percent of the triple point height, the overpressure is significantly greater than expected. At locations approaching the triple point height, the overpressure drops off much faster than expected. As the height of the triple point and ground range increases, the overpressure near the triple point can be expected to drop off because of the weakening of the incident shock and the very great angle of incidence.

Appendix B is a summary of data that supports the finding of the described pressure distribution. This effect of a pressure increase above the ground followed by a decrease is found not only in nuclear data, but also in small ($\frac{1}{2}$ lb. TNT) explosions and larger (1000 lb. Penolite) explosions. The effect is also seen in some of the planar shock data that was done at the University of Toronto. The fact that this effect is found in Mach shocks other than nuclear allows several possible causes to be eliminated. The small HE tests indicate that the effect is not caused by atmospheric inversions, funneling, or defects in the Sachs scaling laws. Between the four types of experiments, a large variation in scale is covered. The shock tube Mach stems may be measured in fractions of an inch, while the HE tests cover a span of several feet and the nuclear data covers a distance of up to several miles. The wide range of scales would seem to indicate that the cause of this effect is not due to atmospheric irregularities of any sort. The cause must lie in the way in which the Mach stem is formed and the resulting pressure changes that occur throughout the life of the phenomenon.

The pressure behind the Mach stem may be found from the following

relation:

$$P_2 = P_1 \left\{ \frac{2 \gamma M_1^2 \cos^2 \psi}{(\gamma + 1) \cos^2(\theta + \psi)} - \frac{\gamma - 1}{\gamma + 1} \right\} \quad (V-4)$$

Where ψ = Instantaneous angle of rise of the triple point

θ = Wedge angle

$\theta = 90$ - angle of incidence for spherical shocks

P_1 = Ambient air pressure

P_2 = Pressure behind the Mach stem

An increase in the angle ψ will always correspond to an increase in the pressure behind the Mach shock. Similarly, when ψ decreases, the pressure behind the Mach stem will decrease. An increase in θ will also cause an increase in the pressure if all other factors are held constant.

Figure 19 is a graph showing how the angle ψ varies experimentally with the wedge angle and Mach number. Because the angle ψ governs the angle at which the incoming air strikes the Mach stem, an increase in translates into an increase in overpressure in the Mach stem at that point. Thus the vertical axis is also related to overpressure in the Mach stem.

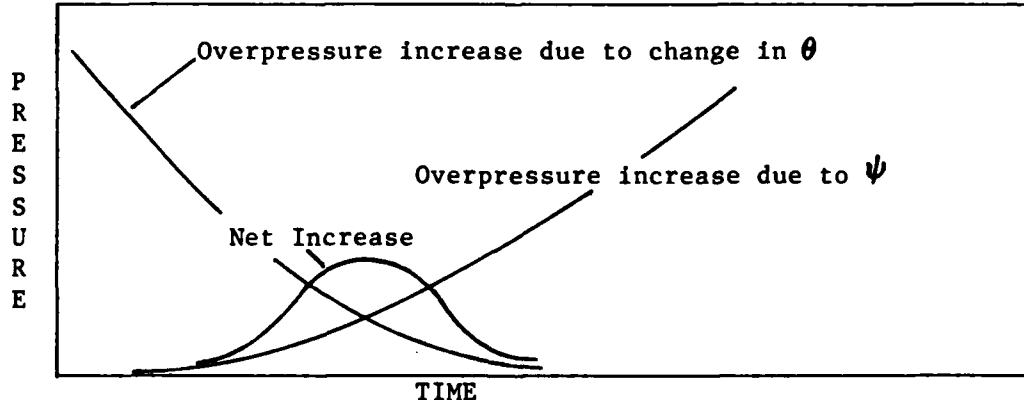


Figure 20. Pressure Increase in the Mach Stem vs. Time

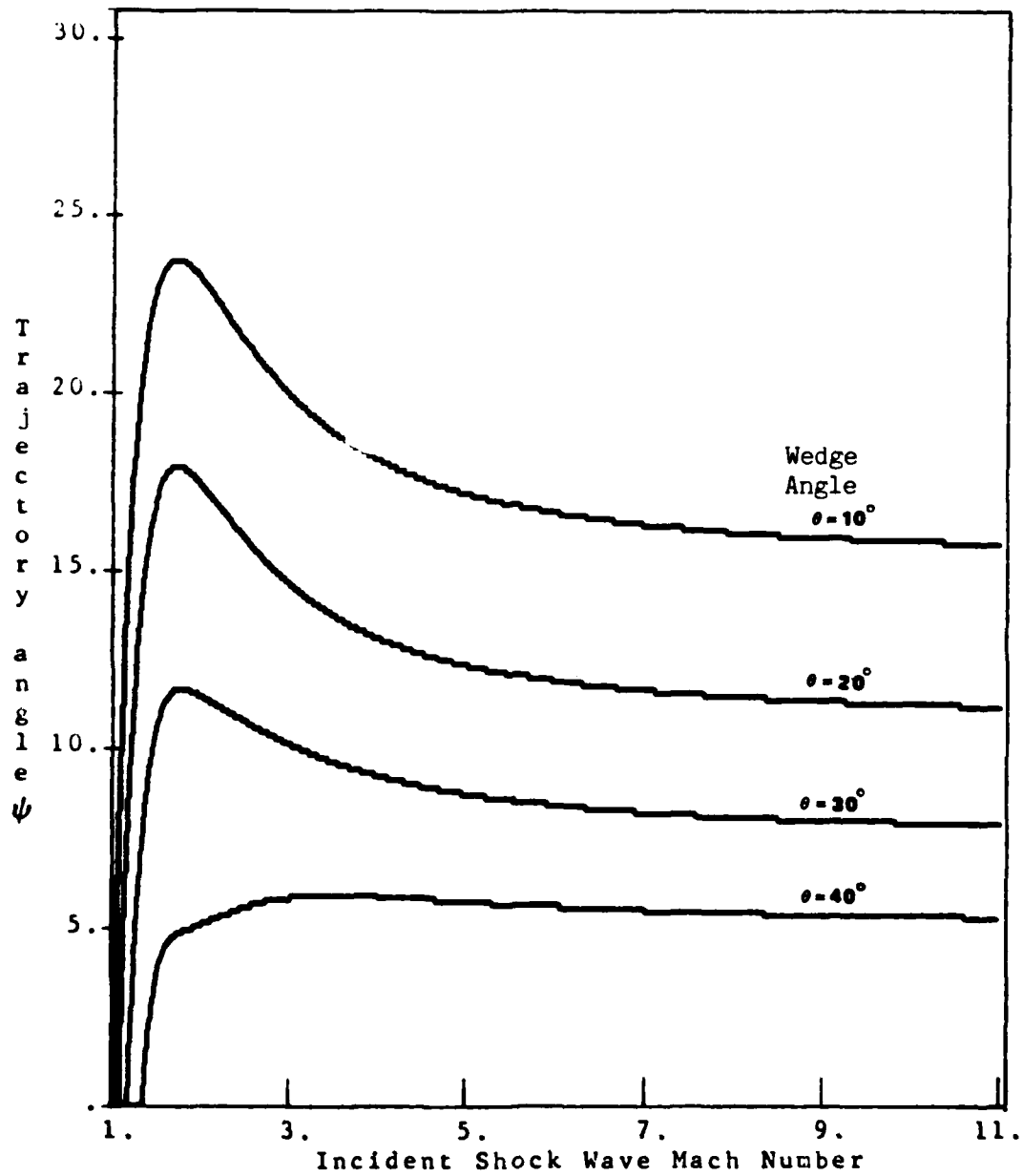


Figure 19. Variation of ψ with Mach Number For Planar Shocks

In a spherical shock, the angle θ will decrease with time due to the rise of the Mach stem. As shown in figure 20, this will cause a gradual decrease in the pressure in the mach stem just below the triple point. The angle ψ will increase with time because the Mach number of the shock decreases with time and because the angle θ is decreasing. This will cause the overpressure just below the triple point to rise (See figure 19). The net result of the two opposing forces is the third curve in figure 20. The overpressure in the mach stem in relation to the overpressure in the incident shock first increases and then decreases. Thus one would expect a 'bulge' in the pressure distribution in the Mach stem. The net effect is to have some overpressure on the ground, an increase in pressure at some height above the surface, and above that a decrease in pressure.

At this point it must be noted that the time of measurement is critical to the measurement of the pressure distribution. At very early times, only a pressure increase would be measured. At very late times, the length of the decrease in pressure will be large in proportion to the length of the Mach stem. At middle times, the region of increase in pressure may be proportionally large and gradually diminish in size. It is also clear that the point at which the maximum overpressure occurs in terms of the fractional distance up the Mach stem changes in time. At the ground distance at which a military planner would require the overpressure, the location of this maximum is not likely to change radically with time.

A nuclear burst is characterized by a spherical symmetry which causes the shock to lose energy relatively rapidly and also allows the angle of

incidence to change with time. Examining the graph of figure 19, it can be seen that at large wedge angles, the amount of increase in ψ is small. Similarly, the amount of increase in small wedge angles is very great. Thus in a low height of burst (200 scaled feet or less) where the triple point rises very rapidly and thus the angle of incidence rises very rapidly (angle of incidence equals $90 - \text{wedge angle}$), it is possible to get a much higher increase in pressure than in a higher height of burst.

With the aid of figure 20, it can be shown that when the Mach stem is generated these variations of pressure exist. With time these pressure variations will tend to diffuse through the shock and equalize the overpressure at all points along the shock front. Whitham has shown that the difference in velocity between two areas of different overpressure will tend to decrease as $t^{-1/2}$ (67:42-47,307-309). Because of the way overpressure is related to shock velocity (See Appendix A), the resulting rate of decrease of the difference in overpressure is somewhat slower. If the magnitude of the overpressure bulge could be predicted, the time it takes to diffuse away could be predicted using the Whitham theory. However, at this time the magnitude of the overpressure bulge is not able to be predicted.

From the nuclear data, a curve fit was made by the author to the data in figure 18. This represents the overpressure profile in the shock after Sachs scaling has been applied. This curve is useful in the region where the profile does not change significantly. It applies only when the height of the triple point has risen to at least twice the height of burst. This region corresponds to overpressures of 20 psi. or less. The

curve was fit by a sixth order polynomial which resulted in the following equation:

$$F = .993766 + 4.72762x - 15.5804x^2 - 21.66193x^3 \quad (V-6) \\ +127.5835x^4 - 155.5353x^5 + 59.9366x^6$$

Where x = Fractional distance up the Mach stem; Target height/HTP

F = Overpressure ratio

The above relation may be used to calculate the overpressure at any given point in the Mach stem by the following relations:

$$\text{Overpressure at altitude} = (\text{ground overpressure})F(P_a)/P_o \quad (V-7)$$

Where F = Overpressure ratio defined above

P_a = Ambient pressure at altitude

P_o = Ambient ground pressure

The overpressure on the ground may be found from any of several relations including the graphs in EM-1, Horizons Technology (51:73-75) and by Brode (8:14-27).

It must be noted that the overpressure distribution as given by equation V-6 is not necessarily the overpressure distribution in the Mach stem at any given instant. It actually represents the variation in pressure that would be seen by a vertical array of gages as the shock wave passed by. Because of the hemispherical shape of the shock wave, the gages on the bottom of the array would be struck first and the topmost ones last. Because the shock wave decays in the small amount of

time between the striking of the lowest and highest gages, the actual overpressure difference in the Mach stem between the top and the bottom may not be as large as the distribution indicates.

In the case of nuclear detonations, there is an additional phenomenon which occurs that may reinforce the rise in overpressure above the surface. The radiation from a nuclear device creates a layer of heated air on the surface of the earth. This situation is similar to and is modeled by a two gas system (See for example ref.36). A light gas such as helium or freon is deposited in such a way that two layers are formed, one layer less dense than the other. When a shock passes through this system, there will be a large increase in overpressure at the boundary between the two layers. It can be shown that this pressure increase occurs in nuclear detonations and that the increase in overpressure above the ground extends far beyond the region of the precursor (See Appendix D for detailed data from several nuclear bursts).

The results of this effect on the overpressure distribution described above is twofold. First, the tendency for the overpressure to rise above the ground is reinforced. In the case of a relatively high height of burst, the overpressure due to this effect will be greater than that due to the change in the angle ψ . Secondly, this increase in overpressure tends to minimize the diffusion of the increased pressure in the shock front in the downward direction. This in turn causes the overpressure profile given above to persist long beyond the times given by the $t^{-1/2}$ decay rate.

Additional, detailed information on this effect may be found in (22:4-103,7), and (45:231-243).

Example Problem

The use of the preceding equations to predict the conditions in the path of an aircraft in flight is shown in the following example. The overpressure, time of arrival, dynamic pressure and gust loading are calculated for an aircraft flying horizontally directly away from the burst at a ground speed of 400 miles per hour (587 feet/sec.). When the shock hits the plane, it is at an altitude of 6,000 feet and a ground range of 20,000 feet. The nuclear burst is one megaton and occurs at an altitude of 3000 feet.

The time of arrival is given by equation V-1:

$$\begin{aligned} \text{Scaled Slant Range, } R &= (\text{Gnd Range}^2 + \text{Altitude}^2) / \text{Yield} \\ &= (20,000^2 + 6000^2) / (1000) = 2,088 \text{ feet} \end{aligned}$$

$$\text{Time of Arrival} = \frac{(.543 - 21.185(2.088) + 361.81(2.088)^2 + 2383(2.088)^3)10}{(1 + 2.04797(2.088) + 2.687(2.088)^2)}$$

$$= 13.7 \text{ seconds}$$

In order to find the overpressure at altitude, the height of the triple point (HTP) and the overpressure on the ground must be known. These two parameters can be found from graphs in EM-1 or from numerical relations such as those given by Potacki. The values given here are from EM-1.

$$\text{Height of the Triple Point, HTP} = 8000 \text{ feet}$$

$$\text{Overpressure on the ground, } dP = 4 \text{ psi.}$$

$$\text{Fractional Distance up Mach stem} = x = \text{Height of Target/HTP}$$

$$= 6000/8000 = .75$$

From equation V-5:

$$\begin{aligned} F &= .993666 + 4.72762(.75) - 15.5804(.75) - 21.66193(.75) \\ &\quad + 127.5835(.75) - 155.5353(.75) + 59.9366(.75) \\ &= .66 \end{aligned}$$

$$\begin{aligned} \text{Overpressure at altitude} &= (\text{Overpr. Gnd})(\text{Tgt. Press})F/14.7 \\ &= 4(.66)11.78/14.7 \\ &= 2.1 \text{ psi.} \end{aligned}$$

The following parameters may be found from U. S. Standard Atmospheres:

Target ambient air pressure = 11.78 psi.

Target ambient air density = .001988 slugs/ft³

Target ambient air sound speed = 1094 feet/sec.

$$\begin{aligned} \text{Airspeed of shock} &= \frac{5(1094)2.1}{7(11.78)(1+6(2.1)/7(11.78))} \\ &= 130 \text{ feet/sec.} \end{aligned}$$

$$\begin{aligned} \text{Effective Radius} &= (.574 + .317(3.) + .0000573(3.)^2)(20,000) \\ &= 30,500 \text{ feet} \end{aligned}$$

$$\begin{aligned} \text{Angle of Shock} &= \tau = \text{Arctan}(\text{Height of Target}/\text{Eff. Radius}) \\ &= \text{arctan}(6000/30500) = 11.13 \text{ degrees} \end{aligned}$$

$$\begin{aligned} \text{Component of shockspeed perpendicular to gnd} &= U_a = U \sin \tau \\ &= 130 \sin(11.13) = 25 \text{ feet/second} \end{aligned}$$

$$\begin{aligned} \text{Component of shockspeed parallel to gnd} &= U_b = U \cos \tau \\ &= 130 \cos(11.13) = 128 \text{ feet/second} \end{aligned}$$

$$\begin{aligned} \text{New Airspeed of Airplane} &= (Ua^2 + (V_1 - Ub)^2) \\ &= (25^2 + (587-128)^2) = 460 \text{ feet/sec.} \end{aligned}$$

$$\begin{aligned} \text{New angle of attack} &= \alpha = \arcsin(Ua/V) \\ &= \arcsin(25/460) = 3.1 \text{ degrees} \end{aligned}$$

$$\begin{aligned} \text{Dynamic Pressure} &= \frac{1}{2} \rho V^2 \\ &= \frac{1}{2} (.002235 \text{ slugs/ft}^3) (460)^2 / 144 \text{ in}^2 / \text{ft}^2 \\ &= 1.6 \text{ psi.} \end{aligned}$$

Comparison With Conventional Predictions.

In order to estimate the effect equation V-7 would have as compared to conventional techniques, a one psi. iso-overpressure contour was plotted for a 500 Kiloton burst with a height of burst of 3175 feet (SHOB = 400 feet). The results for calculations based upon equations IV-6 and IV-7 and conventional techniques are plotted in figure 21. It is clear that the prediction method based upon equations IV-6 and IV-7 is substantially different than the traditional methods of prediction. The overpressure at altitude in the traditional method is a function only of the overpressure on the ground and the pressure at altitude. The proposed predictions are also a function of the fractional distance up the mach stem. There is a large area just below the triple point that is much less dangerous than previously believed. Likewise, nearer the ground, the danger area extends much farther out than before. In this case of the 400 foot scaled height of burst, the danger area extends out nineteen percent farther than the traditional prediction at 3000 feet altitude.

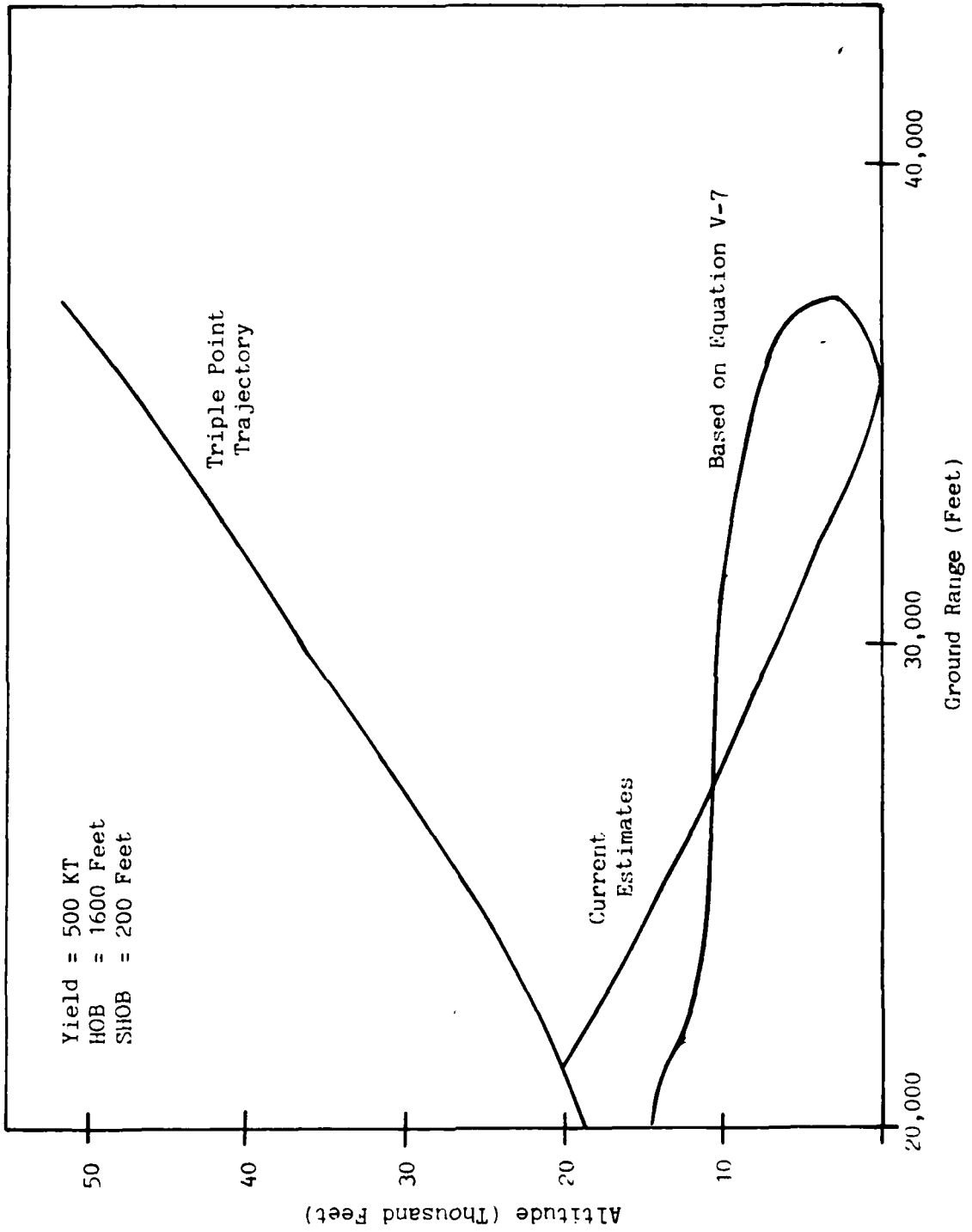


Figure 21. Iso-Overpressure Contour Predictions

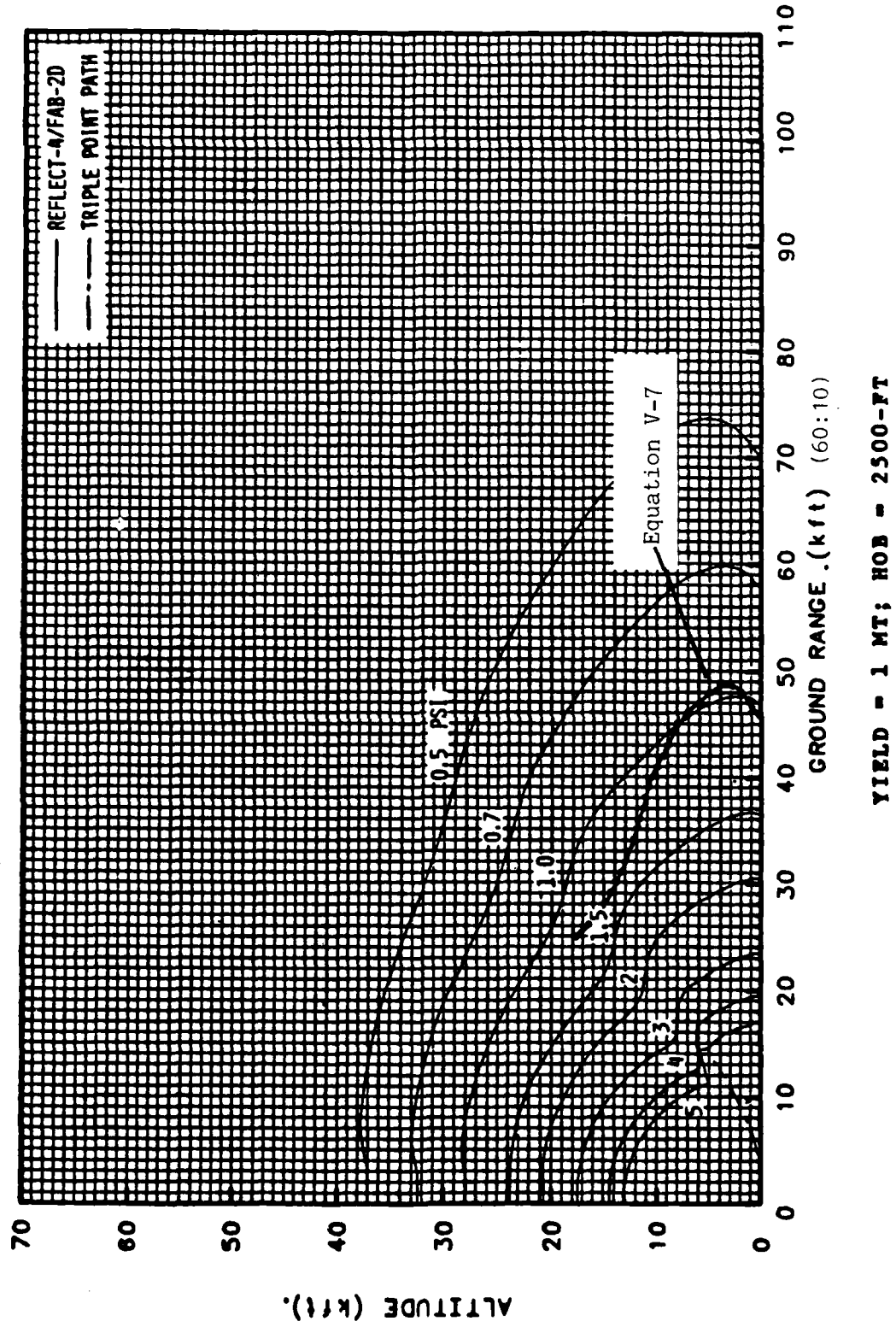
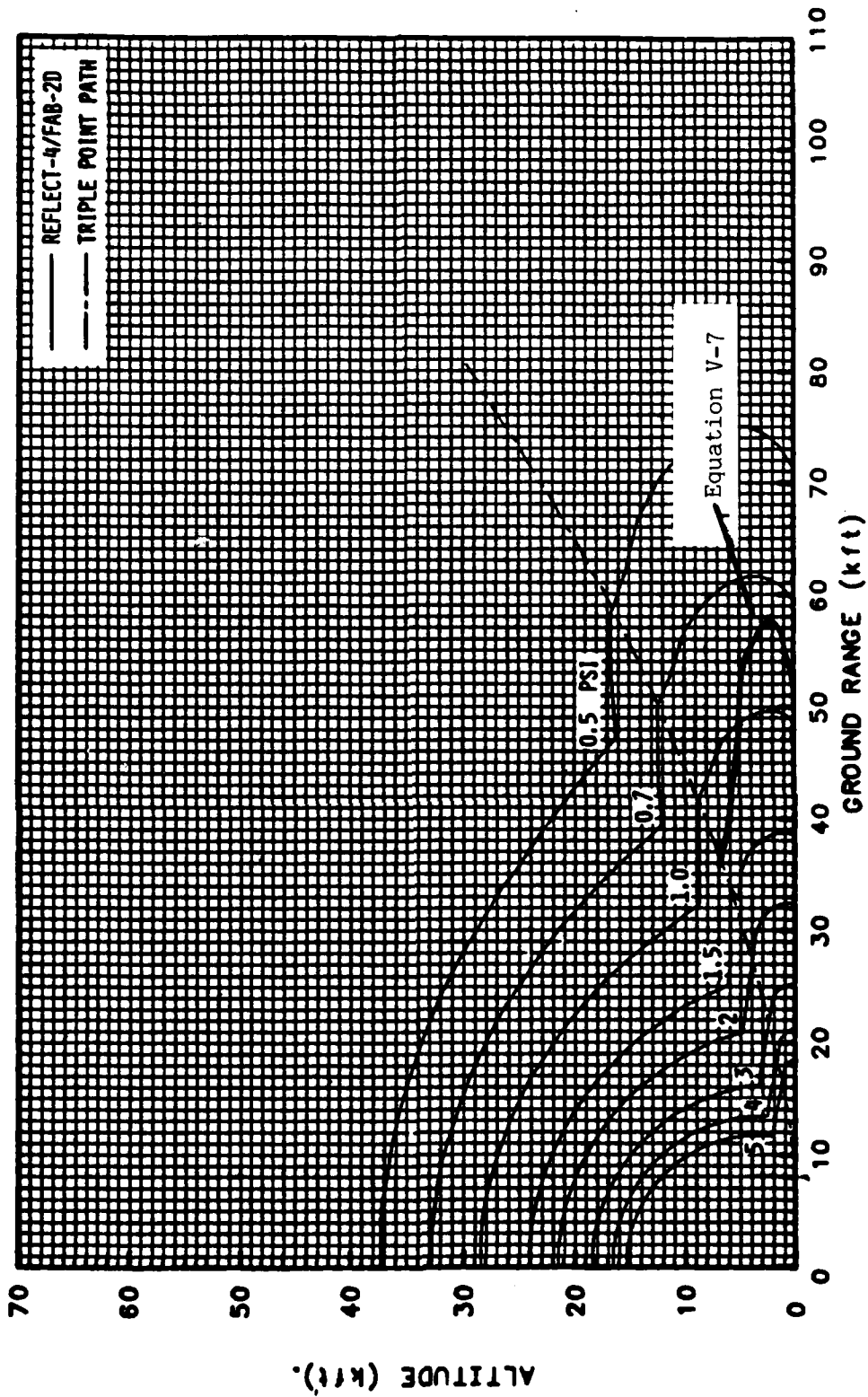


Figure 22. Iso-Overpressure Contour Comparison



YIELD = 1 MT; HOB = 5000-FT (60:11)

Figure 23. Iso-Overpressure Contour Comparison

The Reflect-4 Codes have also predicted the lines of constant overpressure. Two plots are shown as figures 22 and 23. On these figures, the predictions given by equation IV-7 for one psi. are shown. For the one megaton burst at 3000 feet, the two contours show good agreement on the lower half of the contour. The discrepancy between the two predictions is believed to be caused by the codes' values for the angle ψ in this region. The Reflect code predicts a higher angle for in the far regions than other predictions (See (53:figure 6)). This higher value for ψ translates into a higher overpressure in the Mach stem. This also occurs in the second plot for a one megaton burst at 5000 feet. As predicted earlier, the magnitude of the overpressure bulge predicted by equation V-5 is too great for heights of burst greater than 300 scaled feet. In this case, the magnitude of the peak overpressure is about 15 percent too large.

VI. Conclusions and Recommendations

Summary

This paper has used current shock theories augmented by empirical results and new relations, in order to trace the trajectory of the triple point for spherical geometries. Spherical shock configurations were assumed to be instantaneously modeled by planar shocks. This assumption allowed an analytical solution for strong shocks. Curve fits to laboratory data were used when the Mach number of the incident shock dropped below 2. New relations were used for the situation where the triple point is above the burst height.

Empirical relations were developed in this paper for the shape, time of arrival, and overpressure in the Mach stem. These relations used data from measurements taken from free-air nuclear detonations as well as from high-explosive charges of varying sizes. The relations developed here allow the calculation of the overpressure at any altitude in the mach shock if the triple point is at least twice as high as the height of burst.

The iso-overpressure contours given by the relations developed here are markedly different from conventional calculations. They are, however, borne out by the limited nuclear data, and the Reflect-4 Code calculations. The results indicate that near the ground, the iso-overpressure contours extend much farther away from the blast than previously believed. Similarly, the contours near the triple point are much closer to the burst point than before.

Discussion

The finding of a significant departure from traditional predictions has several implications for the military planner and targeteer. The appearance of an area of increased overpressure means that the vicinity of the surface of the ground is more deadly than present predictions show. In the Reflect studies for the Defense Nuclear Agency, it was determined that a pilot in the Mach stem had a choice between climbing to an altitude of lower density (and thus lower overpressure) or diving with the intent of increasing his velocity away from the blast (53:81). The findings here indicate that he should not decrease his altitude. Diving will not only raise the ambient air pressure (and thus the overpressure) but will put the plane closer to the increased overpressure region as well.

An increase in the overpressure above ground means that it is possible to optimize the height of burst to hit targets at some given distance and altitude. In the Base Escape problem, there are many airplanes trying to escape a likely nuclear blast. The probable distribution of these planes in space and time can be determined and targeted to destroy the largest number. Similarly, large buildings can be targeted to place the largest dynamic pressure at some height to inflict the maximum damage. It is important to recognize that maximizing the overpressure on the ground is not the same thing as maximizing the overpressure on some structure of a given height. The 'knee' in the overpressure curves corresponds to the maximum distance that regular reflection can be projected. At this distance the mach stem is not yet formed so that the overpressure against the side of the building is just the free air overpressure and not the

overpressure on the ground.

Recommendations

In order to develop a more efficient and reliable model of the conditions to be found in the Mach stem, two tasks need to be accomplished. First, there must be more measurements made in the Mach stem region above the surface. This will give a better estimate of the magnitude of the overpressure increase for varying heights of burst and the way it propagates in space. This data is crucial to test any formulation purporting to predict conditions in the Mach stem. At present, the data does not cover a wide range of burst heights and distances well or consistently.

Secondly, some type of analytical technique must be developed to predict the overpressure in the Mach stem at distances far below the triple point. At present, theory predicts only the overpressure at some infinitesimal distance below the triple point. Knowing the overpressure variation with altitude, one must be able to predict the manner in which the shock will propagate in space. The shock will clearly deform. This is important to the calculation of gust loading of airfoils. The overpressure bulge will tend to diffuse and equalize the pressure in the shock throughout the front. This means the magnitude of the increase in overpressure will change with time. The only way known to this author of predicting the manner in which this kind of system will propagate is the Whitham shock ray theory. (67:235). This theory has been used with some success in predicting the effects of broken terrain on shock waves (22:5-100). The result of this would be a more comprehensive compilation of curves by which one could estimate the magnitude and location of the

overpressure bulge at any time and for any height of burst. This information would be of great value to military planners who must plan and protect against such possibilities.

Present methods of predicting Mach stem parameters are clearly inadequate. Until more data is available and properly analysed, Mach stem models will remain inaccurate, unreliable, and limited in usefulness at best.

BIBLIOGRAPHY

1. , Air Blast Measurements. Operation Tumbler-Project 1.4. Report to the Test Director, Aberdeen Md: Ballistic Research Laboratories. December 1952. AD-078547.
2. Aronson, C. J., J. F. Moulton et. al. Free Air and Ground Level Pressure Measurements. Operation Tumbler-Project 1.3 and 1.5. WT-513 (Extract). Washington D. C.: Defense Nuclear Agency. November 1952. AD-A995029
3. Baker, Wilfred E. Explosions in Air. Austin, Texas: University of Texas Press, 1973.
4. Bargmann, V. On Nearly Glancing Reflection of Shocks. OSRD Technical Report 5171. Office of Scientific Research and Development. 1945
5. Ben-Dor, G. Regions and Transitions of Nonstationary Oblique Shock-Wave Diffractions in Perfect and Imperfect Gases. UTIAS Report 232. University of Toronto, Institute for Aerospace Studies. August, 1978.
6. Bleakney, Walker, and A. H. Taub. Interaction of Shock Waves. Reviews of Modern Physics, Vol. 21, Number 4. October, 1949. pp. 584-605.
7. Bradley, John N., Shock Waves in Chemistry And Physics. New York: John Wiley and Sons, 1962.
8. Brode, H. L., Height of Burst Effects at High Overpressures. DASA-2506 Washington D. C.: Defense Atomic Support Agency. July, 1980. AD-874060
9. Browne, Philip R. REZONE A Proposal For Accomplishing Rezoning in Two Dimensional Lagrangian Hydrodynamics Problems. LA-3455-MS. Los Alamos: Los Alamos Scientific Laboratory, 1965.
10. Broyles, C. D. Dynamic Pressure vs Time and Supporting Air Blast Measurements. Operation Upshot-Knothole Project 1.1d. WT-714. February, 1954.
11. Bryant, E. J., Ethridge, N. H., and Keefer, J. H. Measurements of Air Blast Phenomena With Self-Recording Gages. Operation Teapot-Project 1.14b WT-1155. Ballistics Research Laboratories, Aberdeen Proving Ground, Maryland, July 1959. AD-616170

12. Bryant, E. J., R. A. Eberhard and C. N. Kingery. Mach Reflection Over Hard Packed Dirt and Dry Sand. BRL Report 809. Aberdeen Md.: Ballistics Research Laboratory. July 1952. AD-801729.
13. Bryant, E. J., and J. H. Keefer. Basic Airblast Phenomena. Operation Plumbob-Project 1.1. WT-1401. Aberdeen Md.: Ballistics Research Laboratories. no date AD-344935.
14. Condon, E. U. and Hugh Odishaw. Handbook of Physics (Second Edition). New York: McGraw-Hill Book Company, 1967.
15. Courant, R. and K. O. Friedrichs. Supersonic Flow and Shock Waves. New York: Interscience Publishers Inc. 1948.
16. Department of the Army. Nuclear Weapons Employment Doctrine and Procedures. FM 101-31-1. Washington: Department of the Army, 1977.
17. Deschambault, Robert L. Nonstationary Oblique-Shock-Wave Reflections In Air. UTIAS Report 270. University of Toronto, Institute for Aerospace Studies. January 1984.
18. Dewey, J. M. and D. J. McMillin. Photogrammetric Analysis of Multiburst Shots: Mighty Mach IV. Contract Report ARBRL-CR-00515 Aberdeen Md.: Ballistics Research Laboratories.
19. Dolan, Philip J. Capabilities of Nuclear Weapons. SRI, DNA EM-1 Washington D. C.: Defense Nuclear Agency. July 1, 1972
20. Eiseman, Peter R. Numerical Solution of the Fluid Dynamical Equations in Curvilinear Coordinates. AFWL-TR-73-172. Air Force Weapons Laboratory, Kirtland AFB, NM. July 1973
21. Ellis, Paul, D. C. Sachs and P. J. Morris. Nuclear Weapons Blast Phenomena Vol I. DASA-1200-I. Washington D.C.: Defense Atomic Support Agency. March 1971. AD-516107. (SECRET)
22. Ellis, Paul, D. C. Sachs and P. J. Morris. Nuclear Weapons Blast Phenomena Vol II. DASA-1200-II. Washington D.C.: Defense Atomic Support Agency. December 1970. AD-513590. (CONFIDENTIAL)
23. Emmons, Howard W. Fundamentals of Gas Dynamics. Princeton, New Jersey: Princeton University Press, 1958.
24. Ethridge, N. H., J. H. Keefer and C. N. Kingery. Sourcebook for Free-Field Nuclear Environment Data Vol. 5. BRL Report 1494 Aberdeen Md.: Ballistics Research Laboratory. April 1972. AD-520977. (SECRET)

25. , Field Test of a System for Measuring Blast Phenomena by Airborne Gages. Operation Plumbob-Project 1.2. ITR-1402 (Extract) Washington D. C.: Defense Nuclear Agency. February 1980. AD-B951745
26. Fletcher, C. H., A. H. Taub, and W. Bleakney. The Mach Reflection of Shock Waves at Nearly Glancing Incidence. Reviews of Modern Physics. Volume 23 pp 271-286. July 1951
27. Glasstone, Samuel and Philip J. Dolan. The Effects of Nuclear Weapons. United States Department of Defense, 1977.
28. Handbook for Analysis of Nuclear Weapon Effects on Aircraft. DNA-2048H-1, Vol. I. Washington D. C.: Defense Nuclear Agency. April, 1970. AD-B012992. (LIMITED)
29. Harlow, Francis H. and Anthony A. Amsden. Fluid Dynamics. LA-4700. Los Alamos: Los Alamos Scientific Laboratory, 1971.
30. Haskell, N. A. Measurement of Free Air Atomic Blast Pressures. Operation Teapot-Project 1.1. WT-1101, February, 1958. AD-460280
31. Haskell, N, A. Free Air Atomic Blast Pressure and Thermal Measurements. Operation Ivy-Project 6.11. WT-631. Air Force Cambridge Research Center, Cambridge Mass., August 1963. AD-A363575
32. Haskell, Norman and J. A. Fava. Measurement of Free Air Atomic Blast Pressures. Operation Redwing Project 1.4. WT-1304. Bedford Mass: AF Cambridge Research Center. AD-357971. (SECRET)
33. Haskell, Norman A. and James O. Vann. The Measurement of Free Air Atomic Blast Pressures. Operation Snapper-Project 1.1. WT-511, Feb., 1953. AD-A078574
34. Haskell, Norman A. and Richard M. Brubaker. Free Air Atomic Blast Pressure Measurements. Operation Upshot-Knothole--Project 1.3. WT-715, April, 1954. AD-A995208
35. Hesse, Richard J. and Jack R. Kelso. Mach Shock Formation From a Nuclear Detonation. AFSWP-510. Washington D. C.: Headquarters, Armed Forces Special Weapons Project. March 1955. AD-223189.
36. Johnson, M. R. and M. J. Balcerzak. Modified Atmosphere Effects on Air Blast. Operation Distant Plain, Project 1.09. DASA 2008. Washington D. C.: Defense Atomic Support Agency. November, 1967. AD-825144. (LIMITED)

37. Keefer, J. H. and R. E. Reisler. Multiburst Environment-Similtaneous Detonations Project Dipole West. BRL Report 1766 Aberdeen Md.: Ballistics Research Laboratories. March 1975.
38. Kingery, C. N. and B. F. Pannill. Parametric Analysis of the Regular Reflection of Air Blast. BRL Report 1249. Aberdeen Proving Ground: Ballistic Research Laboratories. June 1964.
39. Law, C. K. Diffraction of Strong Shock Waves by a Sharp Compressive Corner. UTIAS Technical Note 150. University of Toronto, Institute for Aerospace Studies. July, 1970.
40. Lee, J. H. and I. I. Glass. Domains and Boundaries of Pseudo Stationary Oblique Shock-Wave Reflections in Air. UTIAS Report 262. University of Toronto, Institute for Aerospace Studies. June 1982.
41. Leipmann, Hans W. and Allen E. Puckett. Aerodynamics of a Compressible Fluid. New York: John Wiley and Sons Inc., 1947.
42. Los Alamos Scientific Laboratory. A Numerical Calculation of Two Dimensional Lagrangian Hydrodynamics Utilizing The Concept of Space Dependant Time Steps. LA-3324-MS. Los Alamos: Los Alamos Scientific Laboratory, 1965
43. Los Alamos Scientific Laboratory. The Particle in a Cell Method for the Calculation of the Dynamics of Compressible Fluids. LA-3466. Los Alamos: Los Alamos Scientific Laboratory, 1966
44. Mirels, H. Mach Reflection Flow Fields Associated With Strong Shocks. Report SD-TR-83-50. Washington D.C.: Defense Nuclear Agency. 25 July, 1983. AD-A131384.
45. Morris, W. E. et al. Air Blast Measurements. Operation Upshot Knothole-Project 1.1a and 1.2. WT-710. Silver Spring Md: Naval Ordnance Laboratory. August, 1955. AD-514318. (CONFIDENTIAL)
46. Moulton, J. F. and E. R. Walthall. Shock Wave Photography. Operation Teapot-Project 1.2. WT-1102. U. S. Naval Ordnance Laboratory White Oak, Silver Spring, Maryland, 1969. AD-864107
47. Murphy, B. F. Air Shock Pressure-Time vs Distance. Operation Tumbler-Project 19.1a. WT-501. Albuquerque NM.: Sandia Corporation. 1 August, 1952. AD-514321. (SECRET)
48. Needham, Charles E, Martin L. Havens, and Carolyn S. Knauth. Nuclear Blast Standard (1KT). AFWL-TR-73-55. Air Force Weapons Laboratory: Air Force Systems Command, Kirtland AFB, NM April, 1975. AD-762534

49. Naval Ordnance Laboratory. Theoretical Investigation of Nuclear Burst Phenomena. Document No. 69SD7056. Naval Ordnance Laboratory White Oak, Silver Spring, Maryland, 1969. AD-864107
50. Naval Ordnance Laboratory. Hydrodynamic Calculations of the Shockwave From Nuclear Explosions at Sea-level Altitude of Burst. DASA-1361. Naval Ordnance Laboratory, White Oak, Silver Springs, Maryland, September 1962. AD-414630
51. Potocki, M. L. Evaluations of Five Nuclear Effects Programs Developed by Horizons Technology. Thesis, Air Force Institute of Technology. January, 1981. AD-106388.
52. Rollinson, G. W. Airshock Pressure-Time Vs Distance. WT-602 (Operation Ivy). Albuquerque NM: Sandia Corp. No Date AD-356274 (SECRET)
53. Ruetenik J. R. and J. H. Thompson. Reflect Computer Code for Ground Reflected Blast Waves: Vol I Analysis and Results. DNA 3470F-1 Washington D.C.: Defense Nuclear Agency. 21 April, 1975. AD-C003372 (CONFIDENTIAL)
54. Ruetenik J. R. and J. H. Thompson. Reflect Computer Code for Ground Reflected Blast Waves: Vol III Computed Graphical Results. DNA 3470F-3 Washington D.C.: Defense Nuclear Agency. 21 April, 1975. AD-C003373 (CONFIDENTIAL)
55. Sachs, D. C., L. M. Swift and F. M. Sauer. Airblast Overpressure and Dynamic Pressure Over Various Surfaces. WT-1109, Oct., 1957. AD-617182
56. Schreier, Stephan. Compressible Flow. New York: John Wiley and Sons. 1982.
57. Shapiro, Ascher H. The Dynamics And Thermodynamics of Compressible Fluid Flow. New York: Ronald Press Co. 1953.
58. Smiley, Robert F., J. Ruetenik, and Micheal Tomayko. Reflect-4 Code Computations of 40 KT Nuclear Blast Waves Reflected From the Ground. Vol. I, General Results. DNA-TR-81-203-V1. Washington D.C.: Defense Nuclear Agency, November, 1982.
59. Smiley, Robert F., J. Ruetenik, and Micheal Tomayko. Reflect-4 Code Computations of 40 KT Nuclear Blast Waves Reflected From the Ground. Vol. II, Detailed Data and Plots. DNA-TR-81-203-V2. Washington D.C.: Defense Nuclear Agency, November, 1982.
60. Smiley, Robert F., J. Ruetenik, and Micheal Tomayko. Reflect-4 Code Computations of 1 MT Nuclear Blast Waves Reflected From the Ground. Vol. I, Base Escape Phenomenology. Kaman Avidyne Report TR-221, V-1, May, 1984. (DRAFT).

61. Sternberg, Joseph. Triple Shock-Wave Intersections. Physics of Fluids, Vol. 2, Number 2. March-April 1959. pp 179-192.
62. Stoner, R. G. Mach Reflection of Shock Waves From Charges Detonated in Air. Princeton University OD-03. in NDRC Monthly Report Office of Scientific Research and Development. OSRD 4257 Volume 3. October 30, 1944.
63. Swift, L. M., D. C. Sachs and A. R. Kriebel. Air Blast Phenomena in the High Pressure Region. Operation Plumbob-Project 1.3. WT-1403. Stanford Research Institute, Menlo Park, California. December, 1960. AD-611257
64. Takayama, K. Triple Point Trajectory of a Strong Spherical Shock Wave. AIAA Journal, Vol. 19, June 1981. pp. 815-817.
65. Thompson, Philip A. Compressible Fluid Dynamics. New York: McGraw-Hill Book Co., 1972.
66. Von Mises, Richard. Mathematical Theory of Compressible Fluid Flow. New York: Academic Press Inc. 1958.
67. Whitham, G. B. Linear and Nonlinear Waves. New York NY: John Wiley and Sons. 1974.

APPENDIX A

Oblique Shock Relations

The change in state across a shock is found from consideration of conservation of mass, momentum, and energy across a control volume including the shock front. This will give three equations linking temperature, pressure, density, and velocity across the front. The equation of state for air is a fourth equation to link parameters together on the same side of the shock. These equations have been combined in many forms to obtain one set of parameters in terms of any of the others. Several of the most useful in the analysis of this problem have been: (56:160)

$$\frac{P_2}{P_1} = \frac{2\gamma}{\gamma+1} M_1^2 \sin^2 \phi - \frac{\gamma-1}{\gamma+1}$$

$$\frac{\rho_2}{\rho_1} = \frac{V_{n1}}{V_{n2}} = \frac{V_1 \sin \phi}{V_2 \sin(\phi - \delta)} = \frac{\tan(\phi)}{\tan(\phi - \delta)}$$

$$V_{t1} = V_{t2}$$

$$V_1 \cos \phi = V_2 \cos(\phi - \delta)$$

Where: V_1, V_2 are the velocities of the approaching and exiting air

V_{t1}, V_{t2} are the velocity components tangent to the shock

V_{n1}, V_{n2} are the velocity components normal to the shock

ρ_1, ρ_2 are the densities on each side of the shock

ϕ is the angle of incidence

δ is the angle of deflection of the incident air

P_1, P_2 are the pressures on each side of the shock

M is the mach number of the shock

γ is the ratio of specific heats, for air equal to 1.4

Also of use are the Rankine-Hugoniot equations. This set set of equations as commonly written are derived from the above relations for a normal shock. They express the conditions across the shock front in terms of the similar property ahead of the shock and the overpressure. Overpressure is the easiest property of a shock wave to measure and probably the best predicted property of an incident shock from a detonation.

$$W_1 = C_0 \left\{ 1 + \frac{6dP}{7P_1} \right\}^{-1/2}$$

$$\rho_2 = \rho_1 \left\{ \frac{7P_1 + 6dP}{7P_1 + dP} \right\}$$

$$Q = \frac{2.5 dP^2}{7P_1 + dP}$$

$$P_2 = P_1 + dP$$

Where: Q is the dynamic pressure exerted by the shock

C₀ is the ambient air sound velocity

dP is the pressure difference across the shock

All other symbols are the same

APPENDIX B

Mach Stem Overpressure Data

Nuclear Data

Cannister	Amb. Press Psi.	Gnd Dist Feet	Vert. Alt Feet	Overpress. Psi.	Ta Sec.

	Teapot 4	(30:27)			
8	11.60	6069'	6769'	3.78	3.77
9	10.98	5386'	8319'	3.00	3.914
10	10.37	5172'	9819'	1.90	4.469
	Ivy King	(31:27)			
6	7.17	69081'	19550'	.27	58.62
7	11.46	39946'	7050'	.875	29.93
9	10.30	40109'	10000'	.805	30.48
10	10.42	39150'	9700'	.805	30.36
11	9.80	40570'	11400'	.72	31.33
	Upshot-Knothole 9	(34:25)			
7	11.70	34568'	6550'	.255	29.98
10	9.46	52321'	11925'	.11	47.39
15	11.80	27764'	6325'	.37	23.65
18	11.08	34327'	7875'	.235	29.76
19	10.84	36380'	8400'	.22	31.83
20	10.87	38734'	8350'	.205	33.93
	Snapper 5	(33:25,20)			
1	5.89	26157'	32900'	.141	26.99
2	6.14	16754'	25150'	.175	20.52
3	4.83	19579'	32000'	.128	25.81
4	7.66	7235'	14950'	.425	11.58

Cannister	Amb. Press	Gnd Dist	Vert. Alt	Overpress.	Ta
5	4.50	8676'	27750'	.147	23.37
6	6.43	9334'	18500'	.310	16.09
8	5.23	17096'	25250'	.168	24.34
10	8.50	7559'	12760'	.604	9.59
12	11.01	3725'	5500'	2.69	3.05
13	8.94	1345'	9100'	.817	6.28
15	8.60	10515'	13350'	.486	11.68
16	8.34	19727'	19050'	.307	19.17
Snapper 8 (33:26,27,33)					
1	6.45	11135'	21950'	.276	17.13
4	8.94	9053'	13760'	.624	10.17
6	7.52	14549'	18150'	.314	16.55
7	5.54	14717'	25630'	.207	22.13
8	6.63	25815'	21300'	.205	26.59
9	9.22	17596'	12960'	.370	15.73
10	12.19	8016'	5240'	1.38	5.67
11	11.79	9040'	6210'	1.033	6.73
14	9.24	4038'	12900'	.800	6.95
15	11.38	3662'	7200'	3.235	2.74
16	8.85	11479'	14000'	.488	11.78
Plumbob-Owens (25:23)					
A	11.00	9605'	2900'	.75	2.42
B	10.85	9281'	3800'	.94	2.75
D	9.80	7200'	7000'	.65	2.83
Redwing (32)					
Data Available in Reference 32					

Notes: All Owens Alt. are height above ground
All ground distances calculated.

TNT Bursts Above Ground

HOB	Gnd Dist.	HTP	Height of Gage	Overpressure
2.31'	13.67'	3.4'	0.0'	1.43-1.47
"	"	"	.91'	2.18
"	"	"	1.9'	2.18
"	"	"	2.8'	1.8
"	19.67'	7.0'	0.0'	1.29-1.31
"	"	"	.91'	1.81
"	"	"	2.8'	1.54
"	"	"	5.75'	1.40
"	"	"	6.75'	1.2
3.42'	19.67'	3.5'	0.0'	1.54-1.62
"	"	"	.91'	2.02
"	"	"	2.8'	1.64
"	22.67'	4.5'	0.0'	1.43-1.56
"	"	"	.91'	1.98
"	"	"	2.8'	1.58
4.33'	16.67'	1.4'	0.0'	1.84-2.04
"	"	"	.91'	2.22
"	19.67'	1.8'	0.0'	1.74-1.92
"	"	"	.91'	2.44
"	22.67'	2.5'	0.0'	1.67-1.81
"	"	"	.91'	2.13

Notes: All bursts are $\frac{1}{2}$ lb. of TNT
 All data from Stoner (62:31-34)
 Free air data in same tests show a Std. Dev. of 6.5 percent

Project Dipole West Detonations

Shot	HOB	Gnd Dist	HTP	Height of Gage	Overpressure
7	25.46'	60'	7'	0'	27.5
7	25.46'	60'	7'	3'	36.0
8	24.45'	60'	7'	0'	31.5
8	24.45'	60'	7'	3'	34.8
9	15.15'	40'	5'	0'	79
9	15.15'	40'	5'	3'	80
9	15.15'	60'	15+'	0'	35.6
9	15.15'	60'	15+'	3'	33.5
9	15.15'	60'	15+'	10'	52.4
10	14.92'	40'	7'	0'	67.5
10	14.92'	40'	7'	3'	68
10	14.92'	60'	15'	0'	30.8
10	14.92'	60'	15'	3'	30.0
10	14.92'	60'	15'	10'	43

Notes: Shot 7 data (37:143)
 Shot 8 data (37:151)
 Shot 9 data (37:158-9)
 Shot 10 data (37:165-6)
 All shots were 1080 lbs of penolite

Planar Shock Data

	Angle from Wedge	Fract.	Overpr Gnd	Overpr at Gage	Fract
Case 10	Mach No. 1.66	Wedge Angle =40	=3.3		
1		.303	6.33	7.48	1.2
Case 11	Mach No. 1.90	Wedge Angle =40	=3.8		
1		.263	8.92	12.04	1.34
3.5		.92	9.35	8.41	.89
Case 12	Mach No. 2.41	Wedge Angle =40	=4.4		
1		.227	12.86	18.67	1.45
3.5		.795	13.44	11.62	.76
Case 13	Mach No. 2.87	Wedge Angle =40	=4.5		
1		.222	24.20	29.86	1.24
3.5		.77	24.58	18.78	.76

Notes: Data from ref. 17 table 3, figures 9 and 10.
 Ground overpressures are interpolated from measurements
 1.33 cm apart

APPENDIX C
Origin of the Triple Point Data

HIGH EXPLOSIVE TESTS

HOB	Shock Strength	Gnd Range	Extreme Angle
.5'	.0085	.417'	39.80
1.0'	.02280	.833'	39.80
1.25'	.03306	1.000'	39.667
1.50'	.04858	1.250'	39.80
2.00'	.07842	1.667'	39.80
3.00'	.17464	2.500'	39.80
4.00'	.30225	3.458'	40.85
5.00'	.43867	4.458'	41.72
6.00	.56994	5.916'	44.60

Data From Bryant (12:17)

The above data was collected from 1 lb. TNT bursts over hardpacked earth and dry sand. It should be noted that while the trajectories of the triple points were different for earth and sand, the origins of the triple points are the same within the limits of measurement (12:16).

NUCLEAR EXPLOSIVE TESTS

Shot	HOB	Gnd Range	OverPress.	Strength	Extreme Angle
Teapot 4	500'	550'	200	.07	47.8
Teapot 6	500'	450'	162	.08	42.0
Teapot 8	500'	340'	450	.03	34.2
Teapot 12	400'	325'	450	.03	39.1
Tumbler 1	793'	497'	2.4	.86	32.07
Tumbler 2	1109'	749'	4.97	.747	34.03
Tumbler 3	3447'	2030'	5.77	.71	30.63
Priscilla	700'	550'	366	.038	38.2

Teapot Data (46:50,56,64,86)
 Tumbler Data (2:56)
 Priscilla Data (63:62)

The ground range to the OTP in some cases is estimated. It should be noted that different measurement techniques often give conflicting results. Because of the precursor, gage data is unreliable and photographs may be obscured by dust and debris.

APPENDIX D

Near Ground Overpressure Data

Terrain	Gnd Dist	Height	Overpr	Terrain	Gnd Dist	Height	Overpr
Teapot 12 (55:46-51)							
Water	2000'	0'	17.4	Water	2500'	0'	11.8
	2000'	3'	20.1		2500'	3'	13.2
	2000'	10'	18.1		2500'	10'	12.9
Water	3000'	0'	8.76		2500'	25'	13.7
	3000'	3'	10.5		2500'	40'	11.2
Desert	2000'	0'	16.9	Asphalt	2500'	0'	6.6
	2000'	3'	18.6		2500'	3'	8.5
	2000'	10'	21.9		2500'	10'	6.32
					2500'	25'	6.9
					2500'	40'	6.8
Tumbler 4 (1:44)							
	7300'	0'	2.17		5000'	0'	3.82
	7300'	10'	2.17		5000'	10'	3.85
	7300'	50'	2.17		5000'	50'	3.88
Upshot Knothole 9 (45:64,65,66) Classified							

APPENDIX E

Nuclear Explosion Parameters

The data presented here is a summary of the nuclear explosions that were of use in this analysis. It must be recognized that all of the data presented here is not unquestioned, particularly the given yields. Different references may report substantially different yields, heights of burst, and surface pressures.

Title	Yield	HOB	Scal HOB	Press. Gnd	Alt. Gnd	Ref.
U-K 9	26	2423'	763'	13.05	4191'	(10:78)
Tumbler 1	1.05	793'	747'	13.26	--	(2:202)
Tumbler 2	1.15	1109'	995'	12.73	--	(2:202)
Tumbler 3	30	3447'	1012'	11.17	--	(2:202)
Tumbler 4	19.6	1040'	363'	12.72	--	(2:202)
Priscilla	36.6	700'	201.7'	13.12	3078'	(13:29)
Owens	9.7	500'	222'	12.60	--	(13:29)
Teapot 4	43	500'	135'	12.60	4491'	(46:17)
Teapot 6	7.76	500'	240'	12.71	4245'	(46:17)
Teapot 8	14.23	500'	195'	12.58	4309'	(46:17)
Teapot 12	22.0	400'	137'	13.18	3077'	(46:17)
Ivy King	550	1500'	183'	14.68	0.0'	(31:20,45)
Snapper 5	11.7	300'	126'	12.78	4200'	(33:35)
Snapper 8	14	300'	118'	12.68	4200'	(33:35)

APPENDIX F

Program Description

A program was written using the techniques described in this paper to predict the conditions in the path of the mach stem. It is written in BASIC for a Texas Instruments computer. The language is a standard BASIC except for the way that subroutines are called. Subroutines are CALLED just as in FORTRAN using a parameter list to pass variables. Exits from a subroutine are accomplished using a SUBEXIT or a SUBEND statement. This program is intended to be a subroutine of a much larger program for general predictions from nuclear bursts. The program is called, passing the values for the scaled ground range (SGR), scaled height of burst (SHOB), scaled height of the target (SHT), the ambient pressure at the ground (PG), and the pressure at the target (PT). The parameters returned are the dynamic pressure (Q), the overpressure at the target (OPT), and the angle of the dynamic impulse (TAU).

There are four main subroutines to the program. They are TPLPT, GNDOVERPR, TGTOVERPR, and DYNAMICPR. Of these, TPLPT, which calculates the triple point trajectory, is the largest. TPLPT has a main calling routine that starts at a ground range in the regular reflection region and works its way outward, calculating the value of ψ and the height of the triple point as it goes. The ground range is stepped in increments of five percent of the scaled height of burst until the ground range of the target is exceeded. On this last iteration, the height of the triple point at the target ground range is found by interpolation between the

last two values.

The subroutine is based upon knowing the height of the triple point at some ground range. From this information, the slant range to that point can be found. Subroutine OVERPR is called to find the overpressure and mach number of the incident shock at that point. The geometry of the problem allows determination of the angle of incidence. With this information the subroutine PSI is called to find the angle at which the triple point rises. Knowing the step size and the angle, the location in space of the next point can be found. Once two iterations are done, the triple point is found at the next point by integration of equation IV-1. The subroutine INTEG is used to integrate the equation using Simpson's rule.

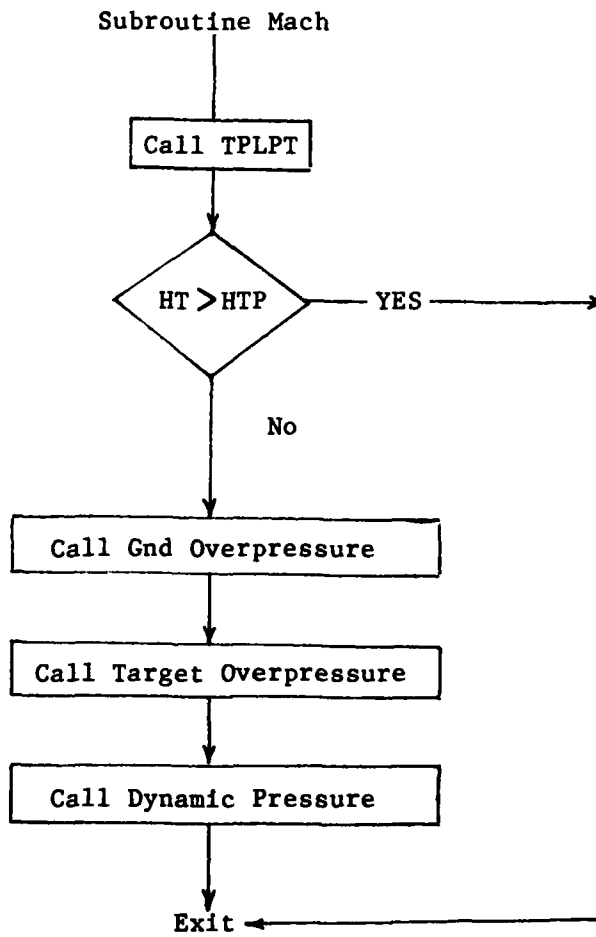
Subroutine PSI uses the techniques outlined in Section IV of this paper. It is divided into three parts. One calculates the angle ψ if the triple point is above the height of burst. The other two are used only when the triple point is below the height of burst and are differentiated by whether the mach number of the incident shock is greater or less than 2.5.

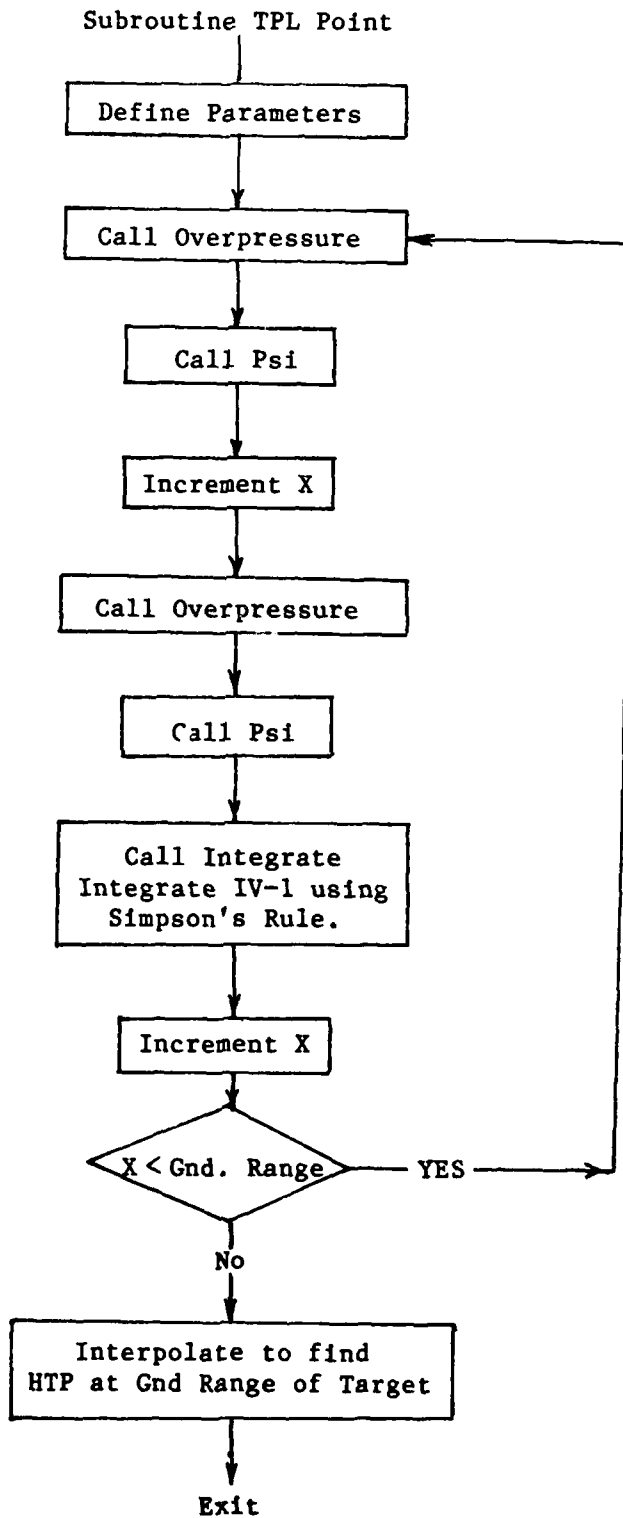
The overpressure on the ground is found by use of the subroutine GNDOVERPR. This routine uses the Horizons Technology version of the EM-1 curves. Input to the program consists of the scaled ground range at which the overpressure is desired and the scaled height of burst. The overpressure on the ground is then returned after being scaled to the ground ambient pressure. This overpressure is then input into the subroutine TGTOVERPR to find the overpressure at altitude. This is found by scaling to the pressure of the target and multiplying by a factor.

This factor is described in the text and describes the pressure variation with height.

The last of the routines is the calculation of the dynamic pressure. This is done by the use of the Rankine-Hugoniot equations. The angle of the impulse is also found. This is found through the estimate of the mach stem radius as described in the text. This angle is used to find the effective angle of attack in the gust loading of an airfoil.

FLOW DIAGRAM





```

100 !*****
110 !***          SUBROUTINE MACH          ***
120 !***  CALCULATES THE CONDITION INSIDE ***
130 !***cTHE MACH STEM IN A NUCLEAR BRURST ***
140 !*****
150 SUB MACH(SGR,SHOB,PT,PG,SHT,Q,OPT,TAU)
160 ! SGR---SCALED GROUND RANGE (FEET)
170 ! SHOB---SCALED HEIGHT OF BURST (FEET)
180 ! SHT---SCALED HEIGHT OF TARGET (FEET)
190 ! HTP---HEIGHT OF THE TRIPLE POINT (FEET)
200 ! OPG---OVERPRESSURE ON THE GROUND (PSI)
210 ! OPT---OVERPRESSURE ON THE TARGET (PSI)
220 ! PG----ATMOS. PRESSURE ON THE GROUND (PSI)
230 ! PT----ATMOS. PRESSURE AT THE TARGET (PSI)
240 ! Q-----DYNAMI C PRESSURE (PSI)
250 CALL TPLPT(SGR,SHOB,HTP)
260 IF HT$HTP THEN 290
270 PRINT "TARGET ABOVE THE MACH STEM"
280 SUBEXIT
290 CALL GNDOVERPR(SHOB,SGR,OPG)
300 CALL TGTOVERPR(OPG,OPT,PG,PT,HT,HTP)
310 CALL DYNAMI CPR(Q,OPT,PT,TAU,SGR,SHOB)
320 SUBEND
330 !*****
340 !***          ***
350 !***          TRIPLE POINT ROUTINE          ***
360 !***          ***
370 !*****
380 SUB TPLPT(SGR,SHOB,YT)
390 ! X----GROUND RANGE/HOB
400 ! TH----90-ANGLE OF INCIDENCE
410 ! PSI---ANGLE AT WHICH THE TRIPLE POINT RISES
420 ! M----MACH NUMBER OF THE INCIDENT SHOCK
430 ! DP---OVERPRESSURE OF INCIDENT SHOCK
440 ! YT---TRIPLE POINT HEIGHT/HOB
450 X=0.75
460 X1=SGR/SHOB
470 GAMMA=1.4
480 HOB=SHOB/3.28
490 !*****
500 !***          TRIPLE POINT          ***
510 !***          MAIN PROGRAM ROUTINE          ***
520 !***          ***
530 !*****
540 CALL OVERPR(HOB,X,YT,M,DP)
550 TH=ATN((1-YT)/X)
560 CALL PSI(HOB,X,YT,TH,PSI1,GAMMA,M,DP)
570 X=X+.05

```

```

580 YT1=YT+.05*TAN(PSI1)
590 TH=ATN((1-YT1)/X)
600 CALL OVERPR(HOB,X,YT1,M,DP)
610 CALL PSI(HOB,X,YT1,TH,PSI2,GAMMA,M,DP)
620 CALL INTEG(PSI1,PSI2,YT,X)
630 IF X$X 1 THEN 670
640 YT=YT-10*(X-X1)/(YT-YT0)
650 YT=YT*SHOB
660 SUBEND
670 X=X+.05
680 YT0=YT
690 GOTO 540
700 !*****
710 !***                               ***
720 !***           SUBROUTINE INTEGRATE       ***
730 !***                               ***
740 !*****
750 SUB INTEG(PSI1,PSI2,YT,X)
760 ! SUBROUTINE USES SIMPSONS RULE TO INTEGRATE AND FINT YT
770 YT=YT+.05*(TAN(PSIO)+4*TAN(PSI1)+TAN(PSI2))/3
780 PSIO=PSI2
790 SUBEND
800 !*****
810 !***                               ***
820 !***           SUBROUTINE OVERPR         ***
830 !***                               ***
840 !*****
850 SUB OVERPR(HOB,X,YT,M,DP)
860 ! SUBROUTINE USES HORIZONS TECHNOLOGY ROUTINE TO FIND FREE AIR OVERPRESSURE
870 ! M IS FOUND USING RANKINE-HUGONIOT EQUATIONS
880 R1=HOB*(X*X+(1-YT)*(1-YT))$.5
890 DP=EXP(.19*(LOG(R1/1000)))$.2-1.5*LOG(R1/1000)-.1)
900 M=(1+(6*DP)/(7*14.7))$.5
910 SUBEND
920 !*****
930 !***                               ***
940 !***           SUBROUTINE PSI           ***
950 !***                               ***
960 !*****
970 !***                               ***
980 !***           MACH NUMBERS $ 2.5       ***
990 !***                               ***
1000 !*****
1010 SUB PSI(HOB,X,YT,TH,PH,GAMMA,M,DP)
1020 IF TH$0 THEN 1910
1030 IF M$2.5 THEN GOTO 1450
1040 PHL=.8*PH
1050 PH=PI/180+PHL

```

```

1060 PHH=PI/2
1070 K1=(GAMMA+1)/(GAMMA-1)
1080 K2=2*GAMMA/(GAMMA+1)
1090 TT=TAN(TH)
1100 TP=TAN(PH)
1110 K1@=(K1*M*M*COS(TH+PH)C2)/(2/(GAMMA-1)+M*M*COS(TH+PH)C2)
1120 K2@=K2-1/(K1*M*M*COS(TH+PH)C2)
1130 CT=1/TAN(TH)
1140 CP=1/TAN(PH)
1150 COT=1/TAN(PH+TH)
1160 E=((K2*M*M*COS(PH)-1/K1)/(K2*M*M*COS(TH+PH)-1/K1))C2
1170 A1=(CP/K1@-(TT+COT/K1@)/(1-TT*COT/K1@))/(1+CP*((TT+COT/K1@)/(1-TT*COT/K1@))
/K1@)
1180 A2=(K1*K2*(1+K1@*K1@*(TAN(TH+PH))C2))/(K1@*K2@(1+K1*E))-1
1190 A3=(E-1)/(GAMMA*(1+K1@*K1@*(TAN(PH+TH))C2)/(K1@*K2@)-E+1)
1200 DELTA=A1*A1-A2*A3*A3
1210 IF (PHH-PHL)§1E-5 THEN 1300
1220 IF ABS(DELTA)§.00001 THEN 1300
1230 IF DELTA§0 THEN 1270
1240 PHL=PH
1250 PH=PH+MIN(PI/180,(PHH-PH)/2)
1260 GOTO 1090
1270 PHH=PH
1280 PH=(PH+PHL)/2
1290 GOTO 1090
1300 SUBEXIT
1310 !*****
1320 !*** ***
1330 !*** MACH NUMBERS § 2.5 ***
1340 !*** ***
1350 !*****
1360 DATA -679.4273854,44.29925276,-.787886744,-.0075477956,.0004252447,-5.11668
E-6,2.06509E-8,-7.0172E-21
1370 DATA -87.33954,-4.195549,.8139311,-.035075,.000691789,-6.58892E-6,2.46545E-
8,-4.73696E-21
1380 DATA 103.1200447,-6.369145,.026000227,.00615099,-.00017623,1.94109E-6,-7.76
64E-9,2.08813E-22
1390 DATA 18.05405,1.215717896,-.2132145477,.0088911,-.0001684565,1.55164E-6,-5.
61549E-9,5.64009E-21
1400 DATA -651.37515,58.00225446,-2.07974387,.0376534976,-.00035084,1.47679E-6,-
1.54965E-9,-6.23181E-21
1410 DATA -4.38396,-.1800461545,.018402893,-.0006043663,.0000104168,-8.80233E-8,
3.33744E-10,-1.76475E-22
1420 DATA 3382.683563,-269.85455,8.74770105,-.1465537887,.0013232252,-5.97838E-6
,1.01429E-8,-4.32411E-22

```

```

1430 DATA -227.2637,13.76562055,-.3163955817,.0031118296,-5.22245E-6,-1.29688E-7
,7.76104E-10,-1.4341E-21
1440 DATA 0,0,0,0,0,0,0,0
1450 T=(PI/2-TH)*180/PI
1460 E=1/((M*M-1)*7/6+1)
1470 IF EW.15 THEN 1510
1480 RESTORE 1360
1490 DELTA=1 :: EO=0
1500 GOTO 1810
1510 IF EW.3 THEN 1550
1520 RESTORE 1360
1530 DELTA=.15 :: EO=.15
1540 GOTO 1810
1550 IF EW.4 THEN 1590
1560 RESTORE 1370
1570 DELTA=.10 :: EO=.30
1580 GOTO 1810
1590 IF EW.5 THEN 1630
1600 RESTORE 1380
1610 DELTA=.10 :: EO=.40
1620 GOTO 1810
1630 IF EW.6 THEN 1670
1640 RESTORE 1390
1650 DELTA=.10 :: EO=.50
1660 GOTO 1810
1670 IF EW.7 THEN 1710
1680 RESTORE 1400
1690 DELTA=.10 :: EO=.60
1700 GOTO 1810
1710 IF EW.8 THEN 1750
1720 RESTORE 1410
1730 DELTA=.10 :: EO=.70
1740 GOTO 1810
1750 IF EW.9 THEN 1790
1760 RESTORE 1420
1770 DELTA=.10 :: EO=.80
1780 GOTO 1810
1790 RESTORE 1430
1800 DELTA=1E65 :: EO=.9
1810 READ A(1),A(2),A(3),A(4),A(5),A(6),A(7),A(8)
1820 READ B(1),B(2),B(3),B(4),B(5),B(6),B(7),B(8)
1830 A1=A(1)+A(2)*T+A(3)*Tc2+A(4)*Tc3+A(5)*Tc4+A(6)*Tc5+A(7)*Tc6+A(8)*Tc7
1840 B1=B(1)+B(2)*T+B(3)*Tc2+B(4)*Tc3+B(5)*Tc4+B(6)*Tc5+B(7)*Tc6+B(8)*Tc7
1850 PHI=A1+(B1-A1)*(E-EO)/DELTA
1860 PHI=MAX(0,PHI)
1870 PH=PHI*PI/180
1880 SUBEXIT

```

```

1890 !*****
1900 !***          ***
1910 !***          NEGATIVE WEDGE ANGLES          ***
1920 !***          ***
1930 !*****
1940 Y1=-YT
1950 CALL OVERPR(HOB,X,Y1,M1,D2)
1960 F=((DP+14.7)*(7*14.7+DP)/(14.7*(7*14.7+6*DP)))c.5
1970 M1=M1*F
1980 T=ATN((YT+1)/X)
1990 PH=2*ATN((SIN(PI/2+TH)*M1-SIN(PI/2-T)*M)/(COS(PI/2-T)*M-COS(PI/2+TH)*M1))
2000 SUBEND
2010 !*****
2020 !***          ***
2030 !***          GROUND OVERPRESSURE          ***
2040 !***          ***
2050 !*****
2060 SUB GNDOVERPR(SHOB,SGR,OPG)
2070 ! SUBROUTINE USES HORIZONS TECHNOLOGY ROUTINE FOR GROUND OVERPRESSURE
2080 HOB=SHOB/3.28
2090 GRR=SGR/3.28
2100 DELTA=ATN(HOB/GRR)
2110 SLS=SQR(HOBc2+GRRc2)
2120 X=LOG(SLS)
2130 P90=.01*EXP(40.3*(SLSc-.295))
2140 PTH=.001*EXP(31.3*(SLSc-.2136))
2150 DELTAPA=P90-(P90-PTH)*(COS(DELTA))c2
2160 IF SLS=100 THEN 2190
2170 DELTAPR=DELTAPA
2180 SUBEXIT
2190 ALPHA=EXP(.3549*Xc3-6.7133*Xc2+41.468*X-82.819)
2200 BETA=EXP(.25192*Xc4-5.8741*Xc3+50.298*Xc2-185.95*X+248.8)
2210 GAMMA=EXP(.1826*Xc4-4.36786*Xc3+38.6017*Xc2-149.59*X+216.26)
2220 DELPTAPB=((COS(DELTA))c(2*BETA))*((SIN(DELTA))cALPHA)*EXP(GAMMA)
2230 DELTAPR=DELTAPA+DELPTAPB
2240 DELTAPX=DELTAPR*PG/14.7
2250 SUBEND
2260 !*****
2270 !***          TARGET OVERPRESSURE          ***
2280 !*****
2290 SUB TGTOVERPR(OPG,OPT,PG,PT,HT,HTP)
2300 !***          ***
2310 !***          ***
2320 X=HT/HTP
2330 F=.993766+4.72762*X-15.580*Xc2-21.6619*Xc3+127.5835*Xc4-155.5353*Xc5+59.936
6*Xc6
2340 OPT=OPG*F*PT/PG
2350 SUBEND

```

```
2360 !*****
2370 !*** ***
2380 !*** DYNAMIC PRESSURE CALCULATION ***
2390 !*** ***
2400 !*****
2410 SUB DYNAMICPR(Q,OPT,PT,TAU,SGR,SHT)
2420 ! Q IS FOUND FROM RANKINE-HUGONOT EQUATIONS
2430 Q=2.5*OPT/(7*PT+OPT)
2440 H=SHOB/100
2450 RE=(.574+.317*H+.0000573*Hc2)*SGR
2460 TAU=ATN(SHT/RE)
2470 SUBEND
```

VITA

Captain William E. Eichinger was born [REDACTED]
[REDACTED] He received a Bachelor of Science Degree in 1976 from
the United States Military Academy, West Point, New York. Upon
graduation he was commissioned in the United States Army Corps of
Engineers. Since that time Cpt. Eichinger has served in the 15th and the
11th Engineer Battalions. His most recent assignment was the Commander
of the 902nd Engineer Company (FBR). He is a graduate of the Engineer
Officer Advanced Course and is licensed as a professional engineer in the
Commonwealth of Virginia.

Permanent Address: [REDACTED]
[REDACTED]

UNCLASSIFIED

SECURITY CLASSIFICATION OF THIS PAGE

AD-A159214

REPORT DOCUMENTATION PAGE

1a. REPORT SECURITY CLASSIFICATION UNCLASSIFIED		1b. RESTRICTIVE MARKINGS	
2a. SECURITY CLASSIFICATION AUTHORITY		3. DISTRIBUTION/AVAILABILITY OF REPORT Approved for public release; distribution unlimited.	
2b. DECLASSIFICATION/DOWNGRADING SCHEDULE		4. PERFORMING ORGANIZATION REPORT NUMBER(S) AFIT/GNE/85M-6	
4. PERFORMING ORGANIZATION REPORT NUMBER(S)		5. MONITORING ORGANIZATION REPORT NUMBER(S)	
6a. NAME OF PERFORMING ORGANIZATION School of Engineering	6b. OFFICE SYMBOL (If applicable) AFIT/ENG	7a. NAME OF MONITORING ORGANIZATION	
6c. ADDRESS (City, State and ZIP Code) Air Force Institute of Technology Wright-Patterson AFB, Ohio 45433		7b. ADDRESS (City, State and ZIP Code)	
8a. NAME OF FUNDING/SPONSORING ORGANIZATION	8b. OFFICE SYMBOL (If applicable)	9. PROCUREMENT INSTRUMENT IDENTIFICATION NUMBER	
8c. ADDRESS (City, State and ZIP Code)		10. SOURCE OF FUNDING NOS.	
		PROGRAM ELEMENT NO.	PROJECT NO.
		TASK NO.	WORK UNIT NO.
11. TITLE (Include Security Classification) See Box 19			
12. PERSONAL AUTHOR(S) William E. Eichinger, Cpt. US Army			
13a. TYPE OF REPORT MS Thesis	13b. TIME COVERED FROM _____ TO _____	14. DATE OF REPORT (Yr., Mo., Day) 1985 March	15. PAGE COUNT
16. SUPPLEMENTARY NOTATION			
17. COSATI CODES		18. SUBJECT TERMS (Continue on reverse if necessary and identify by block number)	
FIELD	GROUP	SUB. GR.	
18	03		
		Nuclear Explosion Effects Overpressure	
		Mach Stem Dynamic Pressure	
19. ABSTRACT (Continue on reverse if necessary and identify by block number)			
Title: MACH STEM MODELING WITH SPHERICAL SHOCK WAVES			
Thesis Chairman: Leslie L. McKee, Major, USAF Asst. Professor of Nuclear Engineering			
<p style="text-align: right;">Approved for public release: LAW AFR 190-1.  W. E. WOLAVER 19 AUG 85 Dean for Research and Professional Development Air Force Institute of Technology (AFIT) Wright-Patterson AFB OH 45433</p>			
20. DISTRIBUTION/AVAILABILITY OF ABSTRACT UNCLASSIFIED/UNLIMITED <input checked="" type="checkbox"/> SAME AS RPT. <input type="checkbox"/> DTIC USERS <input type="checkbox"/>		21. ABSTRACT SECURITY CLASSIFICATION UNCLASSIFIED	
22a. NAME OF RESPONSIBLE INDIVIDUAL Leslie L. McKee, Major, USAF		22b. TELEPHONE NUMBER (Include Area Code) 513-255-5533	22c. OFFICE SYMBOL AFIT/ENG

A semiempirical model was developed for the treatment of the Mach Stem region of a nuclear burst. This model predicts the conditions that would be observed by an aircraft or missile as well as the limits of this region in space. The model is based upon current shock theory. Where three shock theory fails to accurately predict physical reality, new relations are developed or empirical data used.

Specifically, this model predicts the path of the triple point, the overpressure, dynamic pressure, time of arrival, and direction of the shock impulse above the ground. An explanation of the development of each prediction is made and compared to actual nuclear or high explosive test data. Additionally, a comparison is made between conventional Mach Stem modeling and this model.

Unique to this model is a method of predicting the variation of overpressure with altitude above the ground. For low scaled heights of burst, the overpressure found at an altitude of 20 percent of the triple point height is greater than that on the ground. In addition, the overpressure measured just below the triple point is found to be only 60 percent of the ground pressure scaled to altitude. This prediction is radically different than conventional ground overpressures scaled to atmospheric pressure at altitude. The predictions made by this model are verified by nuclear and high explosive test data.